RMK 45

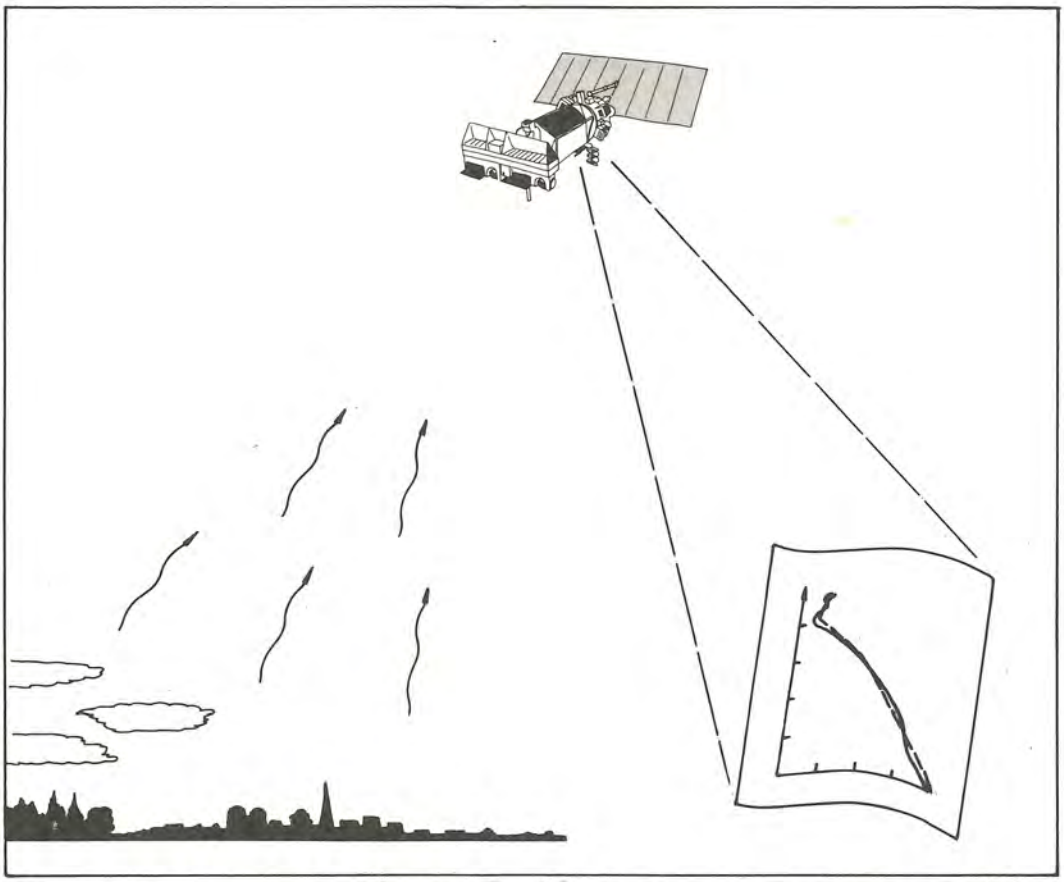

Remote sensing of atmospheric temperature profiles by TIROS Operational Vertical Sounder

Jan Svensson

SMHI SWEDISH METEOROLOGICAL AND HYDROLOGICAL INSTITUTE

SMHI Reports
Meteorology and Climatology

RMK 45

Remote sensing of atmospheric temperature profiles by TIROS Operational Vertical Sounder

Jan Svensson

SMHIs tryckeri, Norrköping 1985

Issuing Agency
SMHI
S-60176 Norrköping
Sweden

Report number
RMK 45

Report date
June 1985

Author (s)

Jan Svensson

Title (and Subtitle)

Remote sensing of atmospheric temperature profiles by TIROS Operational Vertical Sounder

Abstract

A new inversion method for temperature retrievals from satellite soundings is described. The basis of the inversion method is the radiative transfer equation. Surface observations of temperature, humidity and pressure are also included. Basis splines have been used to represent the temperature and humidity profiles. Some physical constraints are also included. This leads to a linear least-squares problem with linear inequality constraints. The extension to a nonlinear least-squares problem is discussed.

The inversion method has been tested with data from TIROS Operational Vertical Sounder in the area 54-61°N, 6-28°E during May, 1983.

Key words

Remote sensing, temperature profiles, splines, inversion methods, satellite meteorology

Supplementary notes

Number of pages
61

Language
English

ISSN and title

0347-2116 SMHI Reports Meteorology and Climatology

Report available from:
SMHI
S-601 76 NORRKÖPING
Sweden

CONTENTS

1. INTRODUCTION

Measurements of temperature, humidity and wind in the atmosphere, have since the second world war been done by radiosondes. In the Northern Hemisphere there are approximately 600 radiosonde stations, making radiosonde launches twice a day. The radiosonde stations are irregularly distributed around the world. The oceans are poorly covered and the Southern Hemisphere is much less covered than the Northern Hemisphere. Temperature and humidity atmospheric profiles, derived from satellite based radiometer data, have become more and more important during the last decade. The global coverage is one good quality of satellite based radiometer measurements. Satellite measurements are important for global, regional and mesoscale weather forecasts.

The TIROS Operational Vertical Sounder (TOVS) is since 1978 flown on the polar orbiting TIROS-N satellites. The calculation of temperature and humidity profiles from radiances received from TOVS includes many problem areas. Some of these are calibration, earth location, cloud contamination, transmittance calculation and inversion methods. Surveys of the problem areas are given in Menzel (1985). In this paper, we will develop a nonlinear, physical inversion method. The inversion method is the process which transforms calibrated, cloud corrected radiances into temperature and humidity atmospheric profiles. We shall concentrate on the temperature retrievals. The humidity profile is in this version of the inversion method a by-product. This part of the inversion method could be developed much more.

The main issues are instrumentation, the radiative transfer equation and modelling the atmospheric temperature profile. These areas are of equal importance in the construction of the inversion method. The three areas are described in Sections 2, 3 and 4 respectively. In Section 5 we develop the inversion method. The approach in the development of our inversion method was

1) efficient and publically available numerical software should be used,
2) the method should be easy to analyse,
3) new ancillary data should be easy to incorporate.

Our inversion method has been inserted in a widely spread software package, TOVS Export Package, developed by the Cooperative Institute for Meteorological Satellite Studies (CIMSS), Madison, Wisconsin. In Section 6 we describe the data processing. Test data are taken from the area 54-61^{o}N, 6-28^{o}E, during the period May 3-26, 1983. Our method is compared to the ordinary inversion method in 'TOVS Export Package'. Test results are presented in Section 7. Some useful symbols and notations are given in Appendix A. We use the technique of singular value decomposition when we analyse the linear system derived from the radiative transfer equation. This is presented in Appendix B. In Appendix C we give more details about that part of the inversion method, which originate from the radiative transfer equation. A scheme for error analysis is suggested in Appendix D. We describe in Appendix E how the nonlinear properties of the radiative transfer equation are handled in the inversion method.

2. INSTRUMENTATION

TIROS Operational Vertical Sounder consists of three instruments. These are the High Resolution Infrared Radiation Sounder (HIRS), the Microwave Sounding Unit (MSU) and the Stratospheric Sounding Unit (SSU). Another instrument, useful for correction of cloud effects on the infrared measurements, is the Advanced Very High Resolution Radiometer (AVHRR). TOVS and AVHRR are flown on the polar orbiting TIROS-N satellites, which have a nodal period of 102 minutes (14.2 orbits per day) and an average altitude of 850 km. The scan geometry of HIRS and MSU is shown in Fig. 2.1. Notice the different horizontal resolution of the HIRS and MSU spots. The different characteristics of the TOVS channels are described in Table 2.1. Carbon dioxide (CO_2) absorbs infrared radiation in the 15 μm band (channel 1-7) and in the 4.3 μm band (channel 13-17). Ozone (O_3) absorbs infrared radiation in the 9.6 μm band (channel 9). Water vapour (H_2O) absorbs infrared radiation in the 6.7 μm band (channel 10-12). Oxygen (O_2) absorbs microwave radiation in a band centered around 60 GHz (MSU channel 1-4). In the window regions (channel 8 and 18-20) the atmospheric absorption is small. This makes the window channels suitable for determination of surface temperature.

More details about TOVS are found in Lauritsen et al (1979), Werbowetzki (1981) and Smith and Woolf (1976). A survey of the predecessors and proposed successors to TOVS is given by Smith (1983).

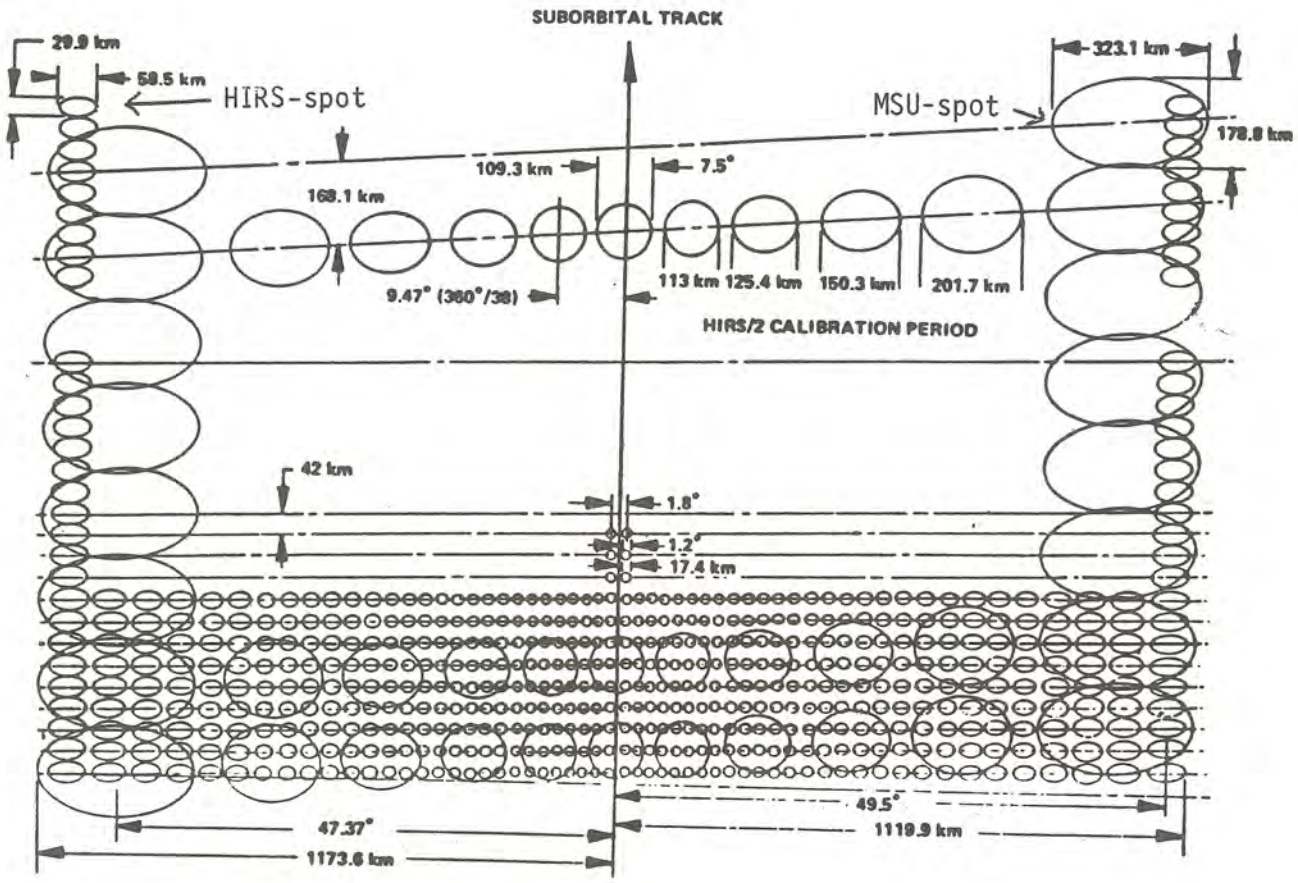

Figure 2.1 TIROS Operational Vertical Sounder HIRS/2 and MSU Scan Patterns Projected on Earth (from Werbowetzki (1981)).

Table 2.1 Characteristics of TOVS channels (from Werbowetzki (1981)).

HIRS Channel number	Channel central wavenumber	Central wavelength (μm)	Principal absorbing constituents	Level of peak energy contribution	Purpose of the radiance observation
1	668	15.00	CO_2	30 mb	*Temperature sounding.* The 15-μm band channels provide better sensitivity to the temperature of relatively cold regions of the atmosphere than can be achieved with the 4.3-μm band channels. Radiances in Channels 5, 6, and 7 are also used to calculate the heights and amounts of cloud within the HIRS field of view.
2	679	14.70	CO_2	60 mb	
3	691	14.50	CO_2	100 mb	
4	704	14.20	CO_2	400 mb	
5	716	14.00	CO_2	600 mb	
6	732	13.70	CO_2/H_2O	800 mb	
7	748	13.40	CO_2/H_2O	900 mb	
8	898	11.10	Window	Surface	*Surface temperature* and cloud detection.
9	1 028	9.70	O_3	25 mb	*Total ozone* concentration.
10	1 217	8.30	H_2O	900 mb	*Water vapor sounding.* Provides water vapor corrections for CO_2 and window channels. The 6.7-μm channel is also used to detect thin cirrus cloud.
11	1 364	7.30	H_2O	700 mb	
12	1 484	6.70	H_2O	500 mb	
13	2 190	4.57	N_2O	1 000 mb	*Temperature sounding.* The 4.3-μm band channels provide better sensitivity to the temperature of relatively warm regions of the atmosphere than can be achieved with the 15-μm band channels. Also, the short-wavelength radiances are less sensitive to clouds than those for the 15-μm region.
14	2 213	4.52	N_2O	950 mb	
15	2 240	4.46	CO_2/N_2O	700 mb	
16	2 276	4.40	CO_2/N_2O	400 mb	
17	2 361	4.24	CO_2	5 mb	
18	2 512	4.00	Window	Surface	*Surface temperature.* Much less sensitive to clouds and H_2O than the 11-μm window. Used with 11-μm channel to detect cloud contamination and derive surface temperature under partly cloudy sky conditions. Simultaneous 3.7- and 4.0-μm data enable reflected solar contribution to be eliminated from observations.
19	2 671	3.70	Window	Surface	
20	14 367	0.70	Window	Cloud	*Cloud detection.* Used during the day with 4.0- and 11-μm window channels to define clear fields of view.

MSU	Frequency (GHz)	Principal absorbing constituents	Level of peak energy contribution	Purpose of the radiance observation
1	50.31	Window	Surface	*Surface emissivity* and *cloud attenuation* determination.
2	53.73	O_2	700 mb	*Temperature sounding.* The microwave channels probe through clouds and can be used to alleviate the influence of clouds on the 4.3- and 15-μm sounding channels.
3	54.96	O_2	300 mb	
4	57.95	O_2	90 mb	

SSU	Wavelength (μm)	Principal absorbing constituents	Level of peak energy contribution	Purpose of the radiance observation
1	15.0	CO_2	15.0 mb	*Temperature sounding.* Using CO_2 gas cells and pressure modulation, the SSU observes thermal emissions from the stratosphere.
2	15.0	CO_2	4.0 mb	
3	15.0	CO_2	1.5 mb	

3. THE RADIATIVE TRANSFER EQUATION

The TOVS measures the upwelling radiation from the earth surface and the atmosphere. The transmittance for a certain frequency denotes the fraction of the radiance from a pressure level, which reaches the satellite. It follows that transmittance is greater than zero and less than one and monotonically increasing with increasing height. The transmittance is associated with the absorption of atmospheric gases (CO_2, O_3, O_2 and H_2O) and is highly varying with frequency. The transmittance for a given frequency at a pressure level depends on water content, ozone content and weakly on temperature between the pressure level of interest and the satellite.

The radiative transfer equation (RTE) for satellite based measurements is (Liou, 1980)

$$I_\nu = \varepsilon_\nu \cdot B_\nu(T_S) \cdot \tau_\nu(P_S) - \int_0^{P_S} B_\nu(T) \cdot \frac{\partial \tau_\nu(P)}{\partial P} \cdot dP \qquad (3.1)$$

where the following notation is used

I_ν radiance at channel 'ν'; $W/(m^2 \cdot sr^1 \cdot cm^{-1})$ ($\tilde{I}_\nu$ is measured radiance),

ν channel number (20 infrared and 4 microwave channels are available on TOVS),

P pressure; mb (P_S is surface pressure),

$T(P)$ temperature; ^oK (T_S is surface skin temperature),

ε_ν emissivity,

$\tau_\nu(P)$ transmittance,

$B_\nu(T)$ Planck function. For the microwave channels $B_\nu(T)$ is linearly proportional to T (Rayleigh-Jean's law).

The dependency of zenith angle is to be understood. Calculation of transmittance is described in Weinreb et al (1981). These calculations are made available through a NOAA software package for 40 different levels from 0.1 to 1000 mb. The 40 levels are shown in Table 3.1. We also define

W(P) water vapour mixing ratio ; g/kg (W_S is surface water vapour mixing ratio),

V(P) ln(W) (V_S is $\ln(W_S)$).

The variables P, T and V are vectorized into vectors $\underset{\sim}{P}$, $\underset{\sim}{T}$ and $\underset{\sim}{V}$ of dimension 'n', where

$n = 40$ if $P_S > 950$ mb,

$n = 39$ if $950 \text{ mb} \geq P_S > 920$ mb,

$n = 38$ if $920 \text{ mb} \geq P_S > 850$ mb

and the sounding is rejected if $P_S \leq 850$ mb.

Table 3.1 The 40 levels for atmospheric computations

Level	Pressure (mb)	Level	Pressure (mb)	Level	Pressure (mb)	Level	Pressure (mb)
1	0.1	11	10	21	115	31	500
2	0.2	12	15	22	135	32	570
3	0.5	13	20	23	150	33	620
4	1.0	14	25	24	200	34	670
5	1.5	15	30	25	250	35	700
6	2.0	16	50	26	300	36	780
7	3.0	17	60	27	350	37	850
8	4.0	18	70	28	400	38	920
9	5.0	19	85	29	430	39	950
10	7.0	20	100	30	475	40	1000

Each element $i < n$ in these vectors correspond to the value of the variables at pressure level 'i', in Table 3.1. The elements p_n, t_n and v_n are P_S, $T(P_S)$ and V_S respectively. The transmittance $\tau(p_n)$ is calculated by linear interpolation (or extrapolation) from the available 40 levels. The surface skin temperature T_S is the temperature at the very thin upper surface layer, while t_n corresponds to the synoptical observations of temperature at 2 m above the ground. There are two reasons for separating t_n and T_S.

1) There is a true difference between the two variables, which may not be neglected. One extreme is the deserts with hot ground during the day and cold ground during the night.

2) The surface emissivity is one parameter in the RTE. However this parameter may not be known exactly. We account for the error in surface emissivity by using separate T_S and t_n. We use the same T_S for all frequencies. This will result in some weighted correction of all emissivity errors in different frequencies.

Each curve in Fig. 3.1 shows the sensitivity of the observed radiance to a variation of atmospheric temperature at different levels. These curves are usually referred to as 'weighting functions'. The weighting functions vary somewhat according to the water vapour and ozone content and also weakly with atmospheric temperature. The different shapes of the curves are related to varying transmittance (or different $\frac{\partial \tau_\nu}{\partial p}$ for different frequencies).

A detailed analysis of the radiative transfer equation and an introduction to atmospheric radiation is found in Liou (1980).

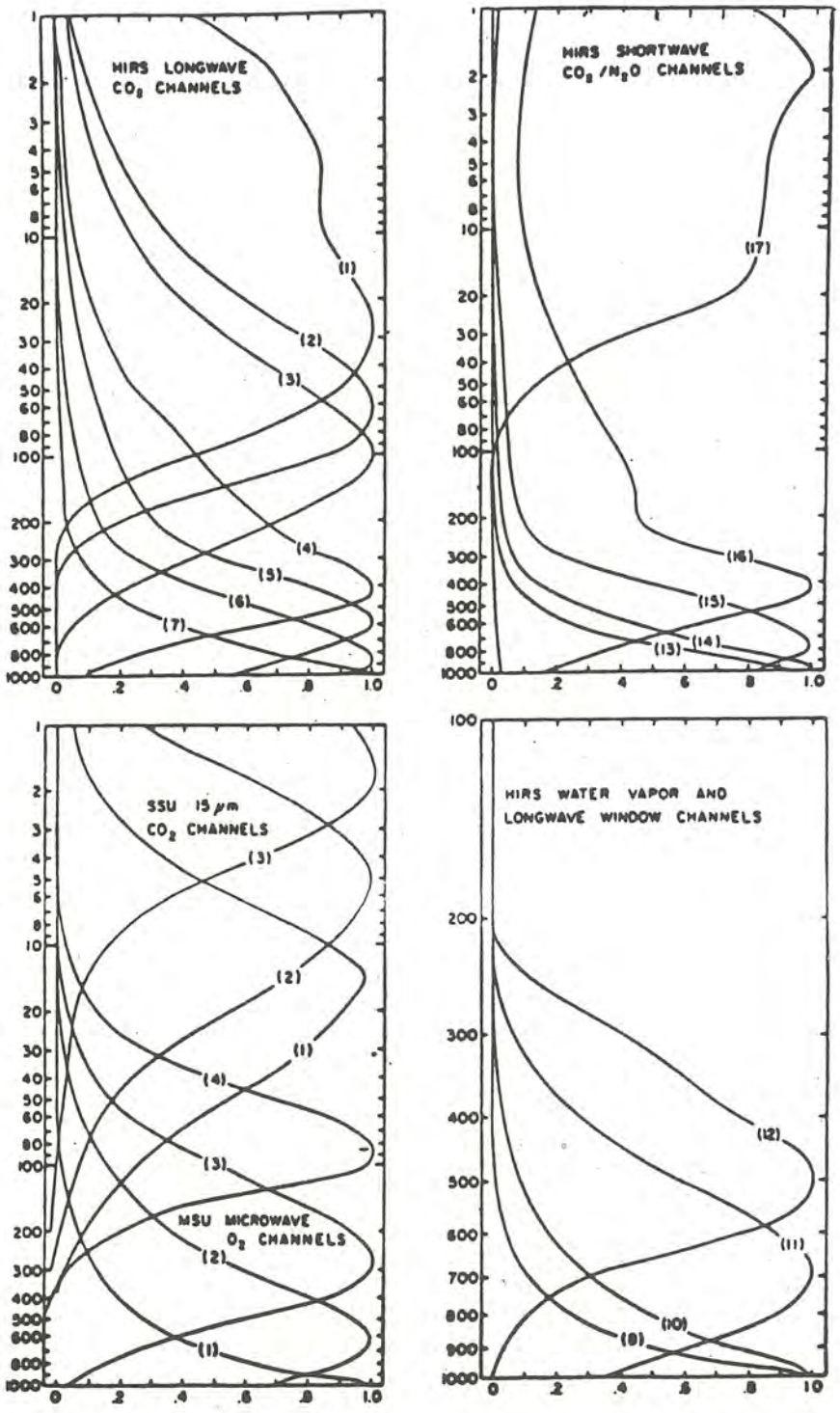

Figure 3.1 TOVS weighting functions (normalized) (from Werbowetzki (1981)).

4. MODELLING THE ATMOSPHERIC TEMPERATURE PROFILE

The use of an appropriate model to describe the atmospheric temperature profile will improve the temperature retrieval from the radiative transfer equation. A necessary condition of a model, is that the modelling error is small compared to the total error in the temperature retrieval from the TOVS-data. Two different models will be analysed; empirical orthogonal functions (EOF-functions) and spline functions.

A quite often used statistical model of many meteorological variables is based upon empirical orthogonal functions, see e.g. Twomey (1977). Given a set of temperature profiles T from 'm' times in one place (or one latitude-longitude zone), a mean temperature profile T_{mean} is calculated. The temperature profile is known for 'n' different pressure levels, $\underset{\sim}{T} = (T(p_1), T(p_2), \ldots, T(p_n))^T$ (m>>n). Calculate

$$\Delta\underset{\sim}{T}^{(j)} = \underset{\sim}{T}^{(j)} - \underset{\sim}{T}_{mean} \quad , \; j = 1, 2, \ldots, m,$$

for each profile $\underset{\sim}{T}^{(j)}$ and define the matrix

$$\Delta\underset{\approx}{T} = (\Delta\underset{\sim}{T}^{(1)}, \Delta\underset{\sim}{T}^{(2)}, \ldots, \Delta\underset{\sim}{T}^{(m)}) \; .$$

The EOF-functions are the eigenvectors $\underset{\sim}{E}_i$, i = 1,2,...,n of the covariance matrix $\Delta\underset{\approx}{T} \cdot \Delta\underset{\approx}{T}^T$, sorted after the size of the eigenvalues in decreasing order. Then every temperature profile $\underset{\sim}{T}$ can be written

$$\underset{\sim}{T} = \underset{\sim}{T}_{mean} + \underset{\approx}{E} \cdot \underset{\sim}{\alpha},$$

where $\underset{\sim}{\alpha}$ is a coefficient vector.

The first eigenvectors are the most important in the approximation of a temperature profile. Eight or ten EOF-functions are often enough to approximate a temperature profile, with an error less than the radiosonde measurement accuracy. Different refinements are possible, like calculating different EOF-functions for different seasons or different types of weather situations. EOF-functions are related to radiosonde data, so their accuracy is depending of location and observation time.

This sensitivity of place and time becomes less pronounced, the more EOF-functions we use in our approximation.

Spline functions, represented by basis splines (B-splines), offer an interesting alternative. A definition of B-splines is found in de Boor (1978). The set of B-splines, used in an approximation, is completely defined by the knots. The twelve cubic B-splines, defined by the knots, which are the logarithms of Ψ_T = {4x10,100,200,300,400,500,600,700,850, 4x1000}, are shown in Fig. 4.1. We will use cubic B-splines and use ln(P) as independent variable. There are several reasons for this choice.

1) Easy and accurate calculation of integrals. This is used in the calculations of layer mean temperature and geopotential thickness. The definition of layer mean temperature between two pressure surfaces P_2 and P_1 ($P_2 > P_1$) is

$$T(P_1,P_2) = \int_{P_1}^{P_2} T(P)\cdot d\ln(P)/(\ln(P_2)-\ln(P_1))$$

and the definition of geopotential thickness Z between two pressure surfaces is (Holton, 1979)

$$Z(P_1,P_2) = R_d/g_o \cdot \int_{P_1}^{P_2} T(P)\cdot d\ln(P).$$

2) Easy and accurate calculation of first derivative $\frac{dT}{d\ln(P)}$. This could be used for a check of dry adiabatic lapse rate (Holton, 1979)

$$\frac{dT}{d\ln(P)} \leq R_d/C_p \cdot T,$$

which may be a useful constraint in the inversion method.

3) Easy and accurate calculation of second derivative $\frac{d^2T}{d(\ln(P))^2}$. This will later on be used in the inversion method as a penalty term (see section 5).

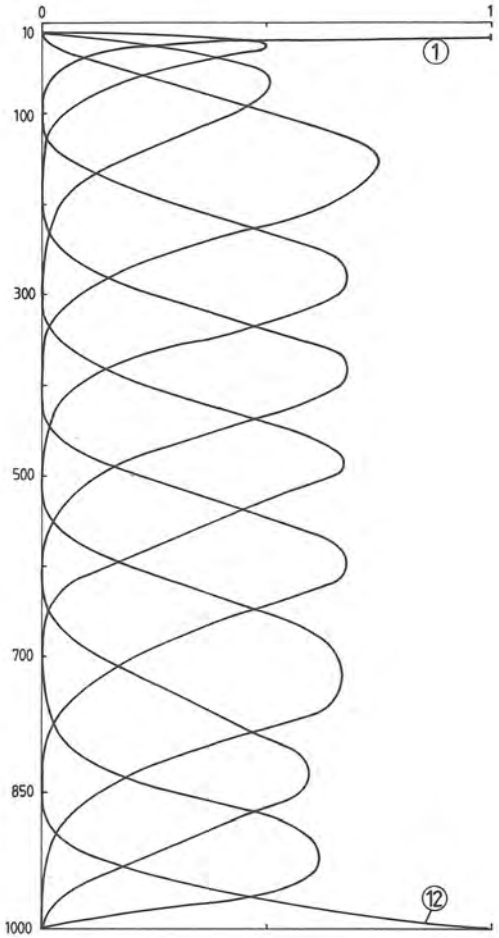

Figure 4.1 The cubic B-splines defined by the knots, which are the logarithms of Ψ_T = {4*10,100,200,300,400,500,600,700,850, 4*1000}

4) If we do not know anything about the function we want to approximate, we may choose equidistant knots. Sometimes we have some information about the function. In those intervals where the function is smooth, we can decrease the number of knots, while we increase the number of knots in those intervals where the function varies more. If we let some knots coalesce, we will have a multiple knot. A multiplicity of two (two knots coalesce) will give a discontinuity in the second derivative at the knot. A multiplicity of three will also make the first derivative discontinuous and a multiplicity of four will make the function discontinuous. A multiple knot could be used for a better approximation of the temperature around the tropopause, where the temperature profile often have a sharp edge.

Spline functions are not related to the existing radiosonde net, so they are more independent of geographical location and observation time than EOF-functions are. Most numerical software libraries offer a number of subroutines for calculations with splines.

The choice of knots may in some cases be important. An interesting approach, used in a problem similar to temperature profile approximation, is given by Holt and Jupp (1978). In their method, the number of knots are fixed but their locations are allowed to change. This will give a nonlinear, least-squares problem which is more complex to solve and requires more CPU-time. We shall not consider this approach any more in this paper.

Test data, for the approximation of temperature profile with EOF-functions and B-splines, are taken from radiosonde measurements at Torslanda (58^{o}N, 12^{o}E) and Sundsvall (62^{o}N, 17^{o}E) in 1971. The radiosonde data from approximately 700 launches for each station have passed certain gross quality checks. The radiosonde temperature profile was then interpolated to twentyone different pressure levels between 100 and 1000 mb. For some of the radiosondes, surface pressure was less than 1000 mb. An extrapolation to 1000 mb was done by assuming a decrease in temperature of 6.5^{o}C/km.

The EOF-functions were calculated from one year of Torslanda data and used for the two separate approximations of Torslanda and Sundsvall data from the same year. We use eleven EOF-functions to solve the least-squares problem

$$\min_{\underset{\sim}{\alpha}} ||\underset{\sim}{\Delta T}^{(j)} - \underset{\approx}{E}^{(11)} \cdot \underset{\sim}{\alpha}||_2,$$

where

$$\underset{\approx}{E}^{(11)} = (\underset{\sim}{E}_1, \underset{\sim}{E}_2, \ldots, \underset{\sim}{E}_{11}),$$

for each profile $\underset{\sim}{T}^{(j)}$. For each pressure p_i, $i = 1,2,\ldots,21$, the error was calculated and a total RMS error was calculated as

$$RMS(p_i) = \left(\sum_{j=1}^{m} (\Delta T^{(j)}(p_i) - \sum_{k=1}^{11} e_{ik} \cdot \alpha_k^{(j)})^2 / m \right)^{1/2},$$

where m is the total number of radiosondes and $\underset{\sim}{\alpha}^{(j)}$ is the least-squares solution derived from profile $\underset{\sim}{T}^{(j)}$.

The result is shown i Fig. 4.2. There is no significant difference in the result from the two radiosonde stations. This implies that if we use as many as eleven EOF-functions, the place, where the EOF-functions are constructed, is not important. The RMS-errors are less than 0.5^{o}K, which is small compared to the accuracy of the radiosondes.

The spline approximation requires that we first choose the knots. The knots were choosen as the logarithms of $\Psi_T = \{4*100, 200, 300, 400, 500, 600, 700, 850, 4*1000\}$ mb. This will give eleven B-splines $B_k(\Psi_T, P)$, $k = 1,2,\ldots,11$ and eleven parameters to calculate. For each profile $\underset{\sim}{T}^{(j)}$ we have to solve the least-squares problem

$$\min_{\underset{\sim}{\beta}} || \underset{\sim}{T}^{(j)} - \underset{\approx}{B} \cdot \underset{\sim}{\beta} ||_2$$

where

$$b_{ik} = B_k(\Psi_T, p_i), \quad i = 1,\ldots,21, \quad k = 1,\ldots,11.$$

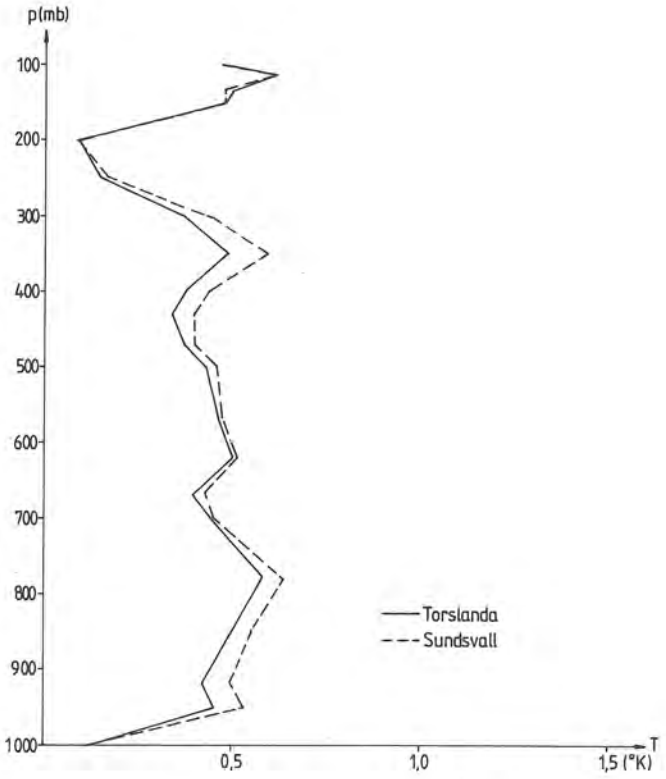

Figure 4.2 RMS-errors in EOF-approximation of temperature profiles from radiosonde measurements.

The RMS-errors were calculated in the same way as for the EOF-functions and shown in Fig. 4.3. We notice that the RMS-errors are approximately of the same order as for the EOF-functions, except in the interval 100-400 mb, where the RMS-errors are considerably higher. This is because of the tropopause which is hard to approximate by spline functions with fixed knots.

Now we could use the property of spline functions to take care of discontinuities in derivatives by using multiple knots. The radiosonde data set contains the pressure at the first tropopause P_{tp}. The first tropopause follows the definition in 'Guide to Climatological Practices, WMO-No-100, TP.44', which says

"The "first tropopause" is defined as the lowest level at which the lapse rate decreases 2^{o}C/km or less, provided also the average lapse rate between this level and all higher levels within 2 km does not exceed 2^{o}C/km."

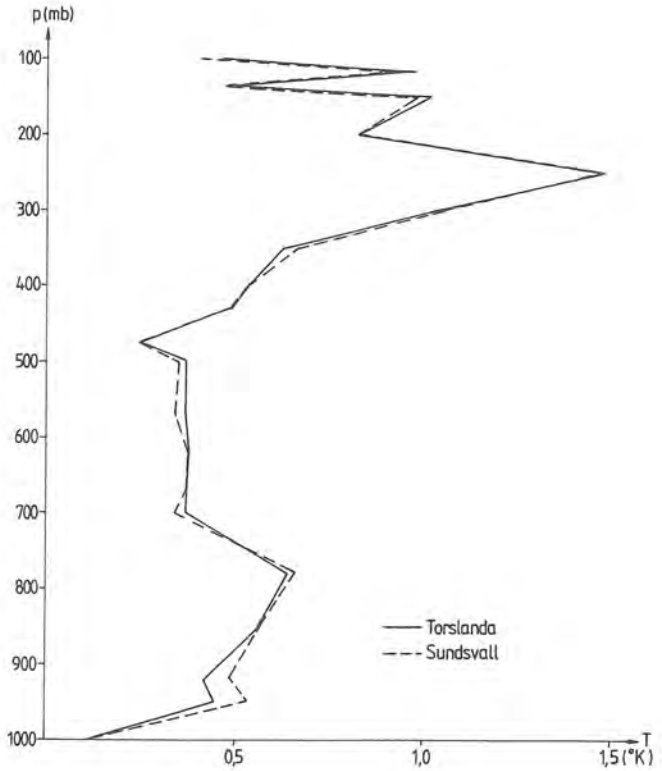

Figure 4.3 RMS-errors in spline approximation, with fixed knots, of temperature profiles from radiosonde measurements.

We place a knot of multiplicity three at the first tropopause. In order to get the same number of parameters to calculate, we delete the first knot with lower pressure than P_{tp} and the first two knots with higher pressure than P_{tp}. If $100 < P_{tp} \leq 200$, then we delete the 200 and 300 mb knots and include a knot of multiplicity two at P_{tp}.

Ex. 1) The first tropopause is 311 mb. Then the inner knots will be the logarithms of 200, 311, 311, 311, 600, 700 and 850 mb.

Ex. 2) The first tropopause is 180 mb. Then the inner knots will be the logarithms of 180, 180, 400, 500, 600, 700 and 850 mb.

Note that this does not imply, that the approximating spline function necessarily will have its first tropopause at the same place as the real tropopause. It is not the optimal choice of the multiple knot we have done, but it is a practical method to choose the knot, and it is believed to be nearly optimal. The RMS-errors are presented in Fig. 4.4.

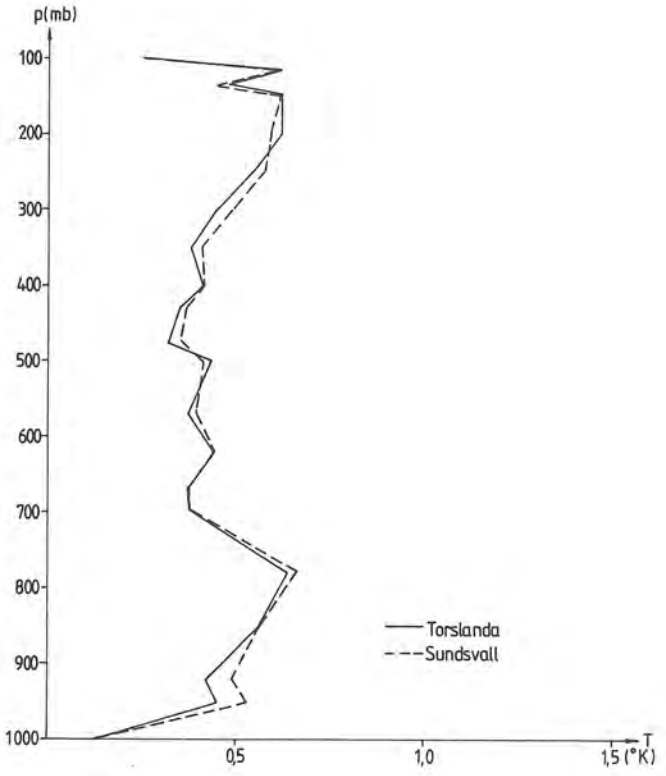

Figure 4.4 RMS-errors in spline approximation, with a multiple knot at the tropopause, of temperature profiles from radiosonde measurements.

This figure shows that we have decreased the error around the tropopause. Now we will have RMS-errors, which for all levels are comparable with those from EOF-functions. This means, that if we have some independent information about the tropopause, we could use it in the inversion method.

The RMS-errors for layer mean temperatures of 100-200, 200-300, 300-400, 400-500, 500-600, 600-700, 700-850 and 850-1000 mb were calculated too. For each, of the three different models used, the RMS errors were less than $0.5^{o}K$ for each layer.

The conclusion will be that, if we use EOF-functions or B-splines with tropopause information, the modelling error in the approximation is small. The error around tropopause may not be neglected for the spline approximation with fixed knots. Because of the excellent approximation properties and publically available numerical software, we prefer to use spline representation of the temperature profiles.

5. INVERSION METHOD

The basis of the inversion method is the radiative transfer equation. Surface observations of temperature, humidity and pressure are also incorporated into the inversion method. B-splines have been used to represent the temperature and humidity profiles. Some physical constraints, represented as linear inequality constraints, are also included. This leads to a linear least-squares problem with linear inequality constraints. Because of the nonlinear properties of the radiative transfer equation, we may have to repeat this process once or twice. This section describes all the parts of the inversion method, which is called THAP (Temperature and Humidity Atmospheric Profiler).

5.1 Taylor expansion of the radiative transfer equation

Suppose we have an initial guess of temperature, surface skin temperature and humidity noted with an upper index '(0)' ($T^{(0)}$, $T_S^{(0)}$ and $V^{(0)}$). The radiance $I_\nu^{(0)}$ is calculated from the RTE with these initial guess values. We assume that the measured radiance $\tilde{I}_\nu$ can be calculated from the RTE with $T^{(0)} + \Delta T$, $T_S^{(0)} + \Delta T_S$ and $V^{(0)} + \Delta V$. We make a first-order Taylor expansion about $T^{(0)}$, $T_S^{(0)}$ and $V^{(0)}$ of the radiative transfer equation and get

$$\begin{aligned} \chi_\nu &\equiv \tilde{I}_\nu - I_\nu^{(0)} \equiv \tilde{I}_\nu - \varepsilon_\nu \cdot B_\nu(T_S^{(0)}) \cdot \tau_\nu(P_S) + \int_0^{P_S} B_\nu(T^{(0)}) \cdot \frac{\partial \tau_\nu(P)}{\partial P} \cdot dP \\ &\approx \frac{\partial I_\nu^{(0)}}{\partial \underset{\sim}{T}} \cdot \Delta \underset{\sim}{T} + \frac{\partial I_\nu^{(0)}}{\partial T_S} \cdot \Delta T_S + \frac{\partial I_\nu^{(0)}}{\partial \underset{\sim}{V}} \cdot \Delta \underset{\sim}{V}. \end{aligned} \tag{5.1}$$

Equation (5.1) may in a shorter form be written

$$\underset{\sim}{Y} = \underset{\approx}{R}_T \cdot \Delta \underset{\sim}{T} + \underset{\sim}{R}_S \cdot \Delta T_S + \underset{\approx}{R}_V \cdot \Delta \underset{\sim}{V} \ , \tag{5.2}$$

where $\underset{\approx}{R}_T$ and $\underset{\approx}{R}_V$ are mxn-dimensional matrices, $\underset{\sim}{R}_S$ is a m-dimensional vector, m is the number of frequencies and n is the number of pressure levels. With $\underset{\sim}{T}^{(0)} + \Delta \underset{\sim}{T}$, $T_S^{(0)} + \Delta T_S$ and $\underset{\sim}{V}^{(0)} + \Delta \underset{\sim}{V}$, we receive better approximations of $\underset{\sim}{T}$, T_S and $\underset{\sim}{V}$. This is the well known Newtons method.

A detailed description of the numerical calculation of $\underset{\sim}{Y}$, $\underset{\approx}{R}_T$, $\underset{\sim}{R}_S$ and $\underset{\approx}{R}_V$ in (5.2) is given in Appendix C.

In order to scale (5.2) properly, each equation, corresponding to channel ν has been multiplied by $1/\frac{\partial B_\nu(B^{-1}(\tilde{I}_\nu))}{\partial T}$. The term $B^{-1}(\tilde{I}_\nu)$ is called brightness temperature. Equation (5.2) together with the equations defined in Section 5.2, will form a system of linear equations, which will be solved as a weighted least-squares problem. The weight we put on each equation is the reciprocal of the assumed error in the equation. The errors in the brightness temperatures, which we estimate in Appendix D, will give the weights of (5.2).

The construction of (5.1) is following the ideas in Smith et al (1985). In their algorithm the integrated amount of precipitable water is used instead of our variable V.

5.2 Ancillary data

Ancillary data are given by surface observations of temperature (T_{OBS}) and humidity ($V_{OBS} = \ln(W_{OBS})$). This will give two equations

$$\Delta t_n = T_{OBS} - t_n^{(0)} \tag{5.3}$$

and

$$\Delta v_n = V_{OBS} - v_n^{(0)} \ . \tag{5.4}$$

The initial temperature profile is given at 'n' levels. However we only allow ΔT to be non-zero for pressure levels up to 10 mb (which corresponds to level 11). This will have the effect, that there is a discontinuity in the temperature profile at 10 mb. This could happen if we allow t_{11} to be changed, but not t_{10}. We require that Δt_{11} should be small. The equation will be

$$\Delta t_{11} = 0. \tag{5.5}$$

The difference between the variables t_n and T_S is assumed to be small. The equation

$$\Delta t_n - \Delta T_S = T_S^{(0)} - t_n^{(0)} \tag{5.6}$$

will express this relation.

The equations (5.3)-(5.6) are weighted, based upon the estimated errors in the variables involved.

5.3 B-splines

We use a set of basis functions, for the variables T and V, instead of discretizing the variables in 'n' levels. This will increase the accuracy of the solution and decrease the number of arithmetic operations. We choose cubic B-splines, with ln(P) as independent variable, to form the basis functions. In Section 4 we showed the approximation properties of B-splines.

We have already mentioned, that we do not allow the temperature to be changed above the 10 mb-level. Besides we do not allow the water vapour to be changed above the 300 mb-level (level 26). This can be expressed in the choice of the knots, which define the B-splines. The knots for the B-splines representing T are the logarithms of $\Psi_T = \{4*10,100,200,300,400,500,600,700,850,4*P_S\}$.

Thus we may express the initial guess temperature profile up to 10 mb as

$$T^{(0)}(P) = \sum_{i=1}^{12} c_i \cdot B_i(\Psi_T,P) \ ,$$

where c_i are spline coefficients for the temperature profile and $B_i(\Psi_T,P)$ is the B-spline 'i' for the given set of knots, Ψ_T, at pressure P. In the same way we will have

$$V^{(0)}(P) = \sum_{i=1}^{9} d_i \cdot B_i(\Psi_V,P)$$

where d_i are spline coefficients for V and $B_i(\Psi_V,P)$ is the B-spline 'i' for the given set of knots, Ψ_V, at pressure P.

The knots for the B-splines representing V up to 300 mb are the logarithms of $\Psi_V = \{4*300,400,500,600,700,850,4*P_S\}$.

We may represent ΔT and ΔV with B-splines in the same way, with the spline coefficients $\underset{\sim}{\Delta C}$ and $\underset{\sim}{\Delta D}$ respectively. Then (5.2)-(5.6) together with the new basis functions will give the linear system

$$\underset{\approx}{R}_T \cdot \underset{\approx}{S} \cdot \underset{\sim}{\Delta C} + \underset{\sim}{R}_S \cdot \Delta T_S + \underset{\approx}{R}_V \cdot \underset{\approx}{U} \cdot \underset{\sim}{\Delta D} = \underset{\sim}{Y} \tag{5.7}$$

$$\underset{\approx}{A}_T \cdot \underset{\sim}{\Delta C} + \underset{\sim}{A}_S \cdot \Delta T_S + \underset{\approx}{A}_V \cdot \underset{\sim}{\Delta D} = \underset{\sim}{Z} \tag{5.8}$$

where the matrices $\underset{\approx}{S}$ and $\underset{\approx}{U}$ in (5.7) have the elements

$$s_{ij} = \begin{cases} 0 & , \quad i = 1,2,....10, \quad j = 1,....12, \\ B_j(\Psi_T, p_i) & , \quad i = 11,12,...n, \quad j = 1,....12, \end{cases}$$

$$u_{ij} = \begin{cases} 0 & , \quad i = 1,2,....25, \quad j = 1,....9, \\ B_j(\Psi_V, p_i) & , \quad i = 26,27,...n, \quad j = 1,....9. \end{cases}$$

The matrices $\underset{\approx}{S}$ and $\underset{\approx}{U}$ may to a large extent be precalculated. They have band structures which are useful (this will decrease the number of arithmetic operations). The non-zero elements of row 11 to 40 in $\underset{\approx}{S}$ are shown for n = 40 in Fig. 5.1.

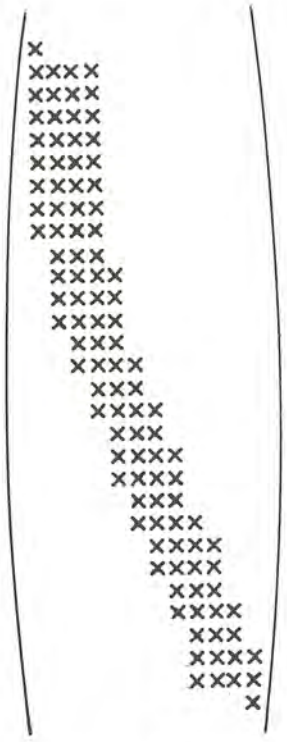

Figure 5.1 Non-zero elements for rows 11,12,...40 for matrix $\underset{\approx}{S}$ (n=40), with the knots chosen as the logarithms of $\Psi_T = \{4*10,100,200,300,400,500,600,700,850,4*1000\}$.

Equation (5.8) is formed by (5.3)-(5.6) and by noting that $\Delta t_n = \Delta c_{12}$, $\Delta t_{11} = \Delta c_1$ and $\Delta c_n = \Delta d_9$. We have

$$\underset{\approx}{A}_T = \begin{pmatrix} 000000000001 \\ 000000000000 \\ 100000000000 \\ 000000000001 \end{pmatrix} ,$$

$$\underset{\sim}{A}_S = (0,0,0\text{-}1)^T ,$$

$$\underset{\approx}{A}_V = \begin{pmatrix} 000000000 \\ 000000001 \\ 000000000 \\ 000000000 \end{pmatrix} ,$$

$$\underset{\sim}{Z} = (T_{OBS} - t_n^{(0)}, V_{OBS} - v_n^{(0)}, 0, T_S^{(0)} - t_n^{(0)})^T .$$

We have a linear least-squares problem with 22 unknowns and m+4 equations. Methods for solving optimization problems, including least-squares problems, are described in Gill et al (1981). The weighted least-squares problem for (5.7) and (5.8) can in short form be written

$$\min_{\underset{\sim}{F}} ||\underset{\approx}{K} \cdot \underset{\sim}{F} - \underset{\sim}{G}||_2, \qquad (5.9)$$

where

$$\underset{\approx}{K} = \underset{\approx}{E} \cdot \begin{pmatrix} \underset{\approx}{R}_T \cdot \underset{\approx}{S} & \underset{\sim}{R}_S & \underset{\approx}{R}_V \cdot \underset{\approx}{U} \\ \\ \underset{\approx}{A}_T & \underset{\sim}{A}_S & \underset{\approx}{A}_V \end{pmatrix} , \quad \underset{\sim}{F} = \begin{pmatrix} \underset{\sim}{\Delta C} \\ \Delta T_S \\ \underset{\sim}{\Delta D} \end{pmatrix} ,$$

$$\underset{\sim}{G} = \underset{\approx}{E} \cdot \begin{pmatrix} \underset{\sim}{Y} \\ \underset{\sim}{Z} \end{pmatrix} .$$

$\underset{\approx}{E}$ is a (m+4) x (m+4)-diagonal matrix, where element e_{ii} is the weight for equation 'i'.

This problem is ill-conditioned, see Twomey (1977), and taking the least-squares solution

$$\underset{\sim}{F} = (\underset{\approx}{K}^T \underset{\approx}{K})^{-1} \cdot \underset{\approx}{K}^T \cdot \underset{\sim}{G} ,$$

will be physically unacceptable, because of the influence of measurement errors in the RTE. In Appendix B we analyse the linear system derived from the RTE, by using singular value decomposition. Numerical algorithms for ill-conditioned problems are surveyed in Björck and Eldén (1979). In order to have a physically acceptable solution, we may add physical constraints and penalty terms.

5.4 Physical constraints

Physical constraints added to an inverse problem may, as a complement to other methods, improve the solution, see Wahba (1982). Here we will use two physical constraints, which are transformed to linear inequality constraints.

The dry adiabatic lapse rate, defined in Holton (1979), is constraining the temperature variations by $\frac{dT}{d\ln(P)} \geq R_d/C_p \cdot T$ where R_d and C_p are constants. With a representation of T in B-splines we will have in terms of the unknown $\Delta\underset{\sim}{C}$,

$$\sum_{i=1}^{12} (B_i'(\Psi_T,P) - R_d/C_p \cdot B_i(\Psi_T,P)) \cdot \Delta c_i \geq$$

$$\sum_{i=1}^{12} (-B_i'(\Psi_T,P) + R_d/C_p \cdot B_i(\Psi_T,P)) \cdot c_i \ .$$

We add these constraints for the pressure levels 26, 27 .... n.

The relative humidity has to be in the interval 0 to 100%. The lower limit is automatically fulfilled, beacuse we use the variable V = ln(W). From the Clausius-Clapeyron equation (see e.g. Hess (1959)), we have

$$W \leq 1000 \cdot \varepsilon/P \cdot e_o \cdot \exp(\varepsilon \cdot L_o/R_d \cdot (1/273-1/T)) \ ,$$

where the constants ε, e_o, L_o and R_d are described in Appendix A. Then

$$V = \ln(W) \leq \ln(1000 \cdot \varepsilon/P \cdot e_o) + \varepsilon \cdot L_o/R_d(1/273-1/T) = \ln(\alpha/P) + \beta(1/273-1/T) \ ,$$

where α= 3800.42 and β = 5418.1185.

This is a nonlinear constraint on V and T. We may linearize it by doing a Taylor expansion about $T^{(0)}$ and $V^{(0)}$. In terms of the unknown $\underset{\sim}{\Delta C}$ and $\underset{\sim}{\Delta D}$ we then have

$$\sum_{i=1}^{9} B_i(\Psi_V,P)\cdot\Delta d_i - \beta/(T^{(0)}\cdot T^{(0)})\cdot \sum_{i=1}^{12} B_i(\Psi_T,P)\cdot\Delta c_i \leq$$

$$\ln(\alpha/P) + \beta(1/273-1/T^{(0)}) - V^{(0)} \ .$$

We add these constraints for the pressure levels 26, 27, ..., n.

5.5 Penalty terms

We will add penalty terms, or regularization functionals, which reflect the supposed behaviour of the solution to the inverse problem. We will require that the variables T and V will be smooth. We then change (5.9) to

$$\min_{\underset{\sim}{F}}\{||\underset{\approx}{K}\cdot\underset{\sim}{F} - \underset{\sim}{G}||_2^2 + \lambda_T\cdot\int_{\ln(10)}^{\ln(P_S)}(T''(P))^2\cdot d\ln(P) + \lambda_V\cdot\int_{\ln(300)}^{\ln(P_S)}(V''(P))^2\cdot d\ln(P)\}, \tag{5.10}$$

where λ_T and λ_V are positive, regularization parameters to be determined (T'' and V'' are short for $\frac{d^2T}{d(\ln(P))^2}$ and $\frac{d^2V}{d(\ln(P))^2}$). A similar penalty term for temperature profiles, where $(\Delta T)''$ is used instead of T'', has been proposed by O'Sullivan and Wahba (1984).

If we use spline representation, we will have

$$\int_{\ln(10)}^{\ln(P_S)}(T''(P))^2\cdot d\ln(P) = (\underset{\sim}{C} + \underset{\sim}{\Delta C})^T\underset{\approx}{Q}(\underset{\sim}{C} + \underset{\sim}{\Delta C})$$

and

$$\int_{\ln(300)}^{\ln(P_S)}(V''(P))^2\cdot d\ln(P) = (\underset{\sim}{D} + \underset{\sim}{\Delta D})^T\underset{\approx}{H}(\underset{\sim}{D} + \underset{\sim}{\Delta D}),$$

where

$$q_{ij} = \int_{\ln(10)}^{\ln(P_S)} B_i'(\Psi_T,P)\cdot B_j'(\Psi_T,P)\cdot d\ln(P) , \qquad i, j \leq 12,$$

and

$$h_{ij} = \int_{\ln(300)}^{\ln(P_S)} B_i'(\Psi_V,P)\cdot B_j'(\Psi_V,P)\cdot d\ln(P), \qquad i, j \leq 9.$$

The matrices $\underset{\approx}{Q}$ and $\underset{\approx}{H}$ can be calculated analytically with few arithmetic operations, they are band matrices with the bandwidth equal to four. Both matrices are symmetric and positive definite. We make a Cholesky factorization, which gives $\underset{\approx}{Q} = \underset{\approx}{L}_T^T\cdot\underset{\approx}{L}_T$ and $\underset{\approx}{H} = \underset{\approx}{L}_V^T\cdot\underset{\approx}{L}_V$ ($\underset{\approx}{L}_T$ and $\underset{\approx}{L}_V$ are triangular matrices).

Now (5.10) is rewritten

$$\min_{\underset{\sim}{F}}\{||\underset{\approx}{K}\cdot\underset{\sim}{F}-\underset{\sim}{G}||_2^2 + \lambda_T||\underset{\approx}{L}_T\cdot\underset{\sim}{\Delta C} + \underset{\approx}{L}_T\cdot\underset{\sim}{C}||_2^2 + \lambda_V||\underset{\approx}{L}_V\cdot\underset{\sim}{\Delta D} + \underset{\approx}{L}_V\cdot\underset{\sim}{D}||_2^2\}, \quad (5.11)$$

which is an ordinary least-squares problem in the unknown $\underset{\sim}{\Delta C}$, ΔT_S and $\underset{\sim}{\Delta D}$. The regularization parameters λ_T and λ_V have to be estimated. We will do a subjective estimation of the parameters. Several different values of these parameters have been tested and those two, which seemed to give the best result were chosen.

In Section 7, we describe how these regularization parameters were chosen in our tests. The regularization parameters were the same during the whole test period, May 1983. We may not assume that the same parameters could be used for all seasons, or even for the same month in another year. In an operational system, we have to automatically compute the optimal (or nearly optimal) regularization parameters. The method of generalized cross-validation, see Craven and Wahba (1979) or Golub et al (1979), determines the regularization parameters from the data (that is in our case from the radiances). The method is developed for non-constrained linear least-squares problems with one regularization parameter. Generalized cross-validation has recently been extended to be used for constrained linear problems by Wahba (1982) and for nonlinear problems

by O'Sullivan and Wahba (1984). The extension to a nonlinear constrained problem with two regularization parameters has to be done.

5.6 Solving the linear least-squares problem subject to linear inequality constraints

We will now solve the linear least-squares problem (5.11) subject to the linear inequality constraints described in Section 5.4. We use the algorithm developed by Stoer (1971). This algorithm also solves least-squares problems with equality constraints. If none of the constraints is active, the computational work in solving the problem, is comparable to methods used for linear least-squares problems without constraints. Stoer's method is an iterative method. We have to choose a starting point which is a feasible point, that is none of the constraints is violated. The constraints of the dry adiabatic lapse rate will cause no problem. An initial guess $T^{(0)}$, which is not too bad, will not violate these constraints. The constraints of the relative humidity might cause more problems. The relative humidity calculated from $T^{(0)}$ and $V^{(0)}$ might be greater than 100% for some pressure levels. We choose $\Delta c_i = 0$, $i = 1,2,\ldots,12$ and $\Delta d_i = -0.1$, $i = 1,2,\ldots,9$ (which will reduce the water vapour mixing ratio with 10%), in order to have a feasible starting point.

5.7 Extension to a nonlinear inversion method

We have now received a better approximation of T, T_S and V, with $T^{(1)} = T^{(0)} + \Delta T$, $T_S^{(1)} = T_S^{(0)} + \Delta T_S$ and $V^{(1)} = V^{(0)} + \Delta V$. With few modifications of the algorithms, we may use $T^{(1)}$, $T_S^{(1)}$ and $V^{(1)}$ as a new initial guess, and repeat the procedure. This will account for the nonlinear properties of the radiative transfer equation. In Appendix E, we show the algorithms with three iterations. In Section 7 we compare the retrieved temperature profiles from one, two and three iterations.

6. DATA PROCESSING

The Physical TOVS Export Package, dated 24 September, 1983 and described by Smith et al (1984), was used. The ordinary inversion method (FXTIRO)

was replaced by our method (THAP). The inversion methods, both FXTIRO and THAP, offer a lot of alternatives. The programs were executed with the following options:

1) Analysed values of surface temperature, surface dewpoint temperature and surface pressure are included.
2) Climate was used as first guess profile. In the lower layers (below 700 mb), it was adjusted after the surface observations. In THAP we use another first guess for the water vapour. We use the formula $W(P) = W_{OBS}*(P/P_S)^3$, which is suggested by Smith (1966) and Hayden et al (1981). In THAP we express temperature and humidity with a spline approximation, see Section 5.3. The spline coefficients are calculated as a least-squares approximation of the adjusted climate.
3) Profiles are produced from 3 x 3 arrays of HIRS spots. This will give an approximate horizontal resolution of 75 km.
4) The high-resolution topography with a horizontal resolution of ten nautical miles was used.

In THAP we use the HIRS-channels 3,4,5,6,7,8,10,11,12,13,14,15 and 16 and the MSU-channels 3 and 4. This will give a total of 15 equations derived from the radiative transfer equation. Surface emissivities for the HIRS-channels are given in Table 6.1, which is taken from Chedin and Scott (1984). Surface emissivity for the MSU-channels is 0.7.

Channel number		7	8	9	10	13	14	18	19
Emissivity	Land	0.98	0.96	0.96	0.93	0.91	0.93	0.88	0.88
	Sea	1.0	0.98	0.98	0.98	0.97	0.98	0.96	0.96

Table 6.1 Surface emissivities for the HIRS-channels. An emissivity of 1 is given to the remaining channels.

The estimated errors in the different equations are given in Table 6.2. The weights are the reciprocals of these errors.

Equation	Error
Derived from RTE for channel 'ν' (5.2)	$1^{o}K$*
Surface observation of temperature (5.3)	$2^{o}K$
Surface observation of humidity (5.4)	0.1**
Temperature at 10 mb (5.5)	$2^{o}K$
Difference between surface temperature and surface skin temperature (5.6)	$3^{o}K$

* Estimated in Appendix D.

** This error in V corresponds to a relative error in W of 10%.

Table 6.2 Estimated errors for each equation used in the inversion method THAP

Three iterations were done for each sounding.

The Physical TOVS Export Package is written in FORTRAN and so is the inversion method THAP. Subroutines from the NAG software library were used for the implementation of the numerical algorithms, with the following major exceptions.

1) The matrices $\underset{\approx}{Q}$ and $\underset{\approx}{H}$ (see Section 5.5) are positive definite matrices. Round-off errors during the calculation of $\underset{\approx}{Q}$ and $\underset{\approx}{H}$ may destroy the property of positive definiteness. The NAG subroutine F01MCF, which makes a Cholesky factorization of positive-definite, variable-bandwidth matrices, failed. The modified Cholesky factorization described by Gill et al (1981) was used instead.

2) The Stoer's method for solving linear least-squares problem with linear inequality or equality constraints was not available in the NAG software library. There was not any other suitable method for this problem in the software library. An ALGOL version, kindly provided by dr Stoer, was rewritten in FORTRAN.

3) The calculation of layer mean temperature includes an integral of spline functions. The algorithm described in de Boor (1978) (page 150-151) was implemented.

7. TESTS

In this Section we will compare the temperature profiles retrieved from our inversion method with the profiles from the ordinary inversion method in 'TOVS Export Package'. We will also show the dramatic improvement, which we will receive when incorporating tropopause information into the inversion method. Finally we compare the retrieved temperature profiles from one, two and three iterations in our inversion method.

Test data are taken from the Meso-scale Analysis Area for PROMIS 600 at SMHI, see Gustafsson and Törnevik (1984), during the period May 3-26, 1983. The ONSAM-experiment gave an opportunity to test the 'TOVS Export Package'. The ONSAM-experiment took place at Onsala Space Observatory ($57^{o}24'$N, $11^{o}55'$E), May 2-26, 1983. The primary objective of this project was to test the performance and profiling capability of ground-based temperature and water vapour microwave radiometers developed at Chalmers University of Technology (Askne, 1984).

During the ONSAM-experiment raw TOVS-data in TIP-format were received from the Danish Meteorological Institute, Observatory for Space Research, Rude Skov, Birkeröd, Denmark, where a read-out station is situated. The implementation of the TOVS Export Package and test results are described by Svensson (1984). The results from the ordinary inversion method, FXTIRO, have now been compared with the results from our method, THAP. Fifteen satellite passages were processed. The test area, with radiosonde stations marked off, is shown in Fig. 7.1. Temperature retrievals from these radiosondes were compared with satellite soundings in the following way.

1) Radiosonde observations at 00Z and 12Z were used. The nearest time to the satellite passage was used. The radiosonde data have passed certain gross quality checks. The satellite and radiosonde soundings are made within four hours of each other.
2) The nearest satellite sounding to each radiosonde was chosen. Distance should be less than 150 km.

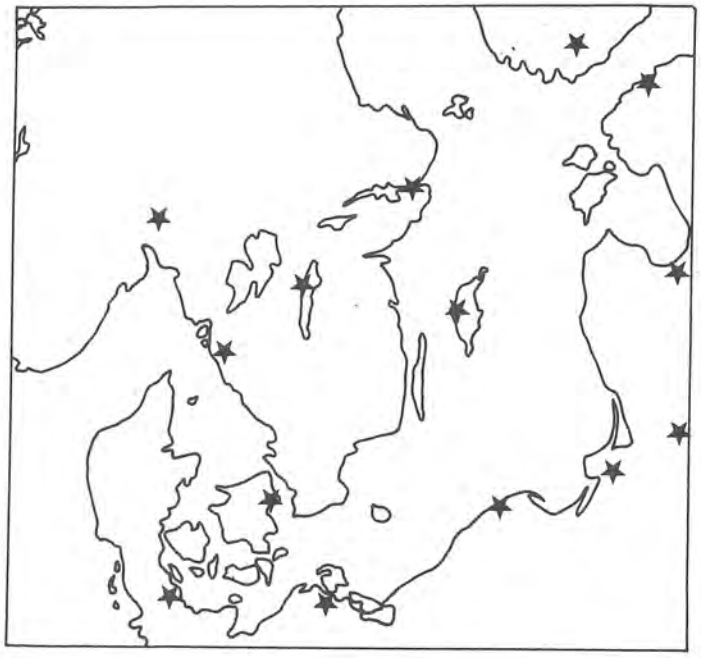

Figure 7.1 Radiosonde stations in the Meso-scale Analysis Area (appr. 54-61^{o}N, 6-28^{o}E)

3) Layer mean temperature for eight levels were calculated and compared. From the definition in Section 4 we see that layer mean temperature can be easily and accurately calculated, with spline representation of the temperature profile. Root-mean-square difference (RMS), standard deviation (STD) and mean difference (MEAN) were calculated. The definitions are

$$RMS = \left(\left(\sum_{i=1}^{k} (TS_i - TR_i)^2\right)/k\right)^{1/2},$$

$$MEAN = \left(\sum_{i=1}^{k} (TS_i - TR_i)\right)/k,$$

$$STD = \left(\left(\sum_{i=1}^{k} (TS_i - TR_i - MEAN)^2\right)/(k-1)\right)^{1/2}$$

where

TS_i = layer mean temperature retrieved from satellite soundings at sample 'i',

TR_i = layer mean temperature retrieved from radiosonde at sample 'i',

k = number of samples.

Only clear retrievals were analysed, because the cloud correction algorithm in this version of TOVS Export Package, was not well adapted for our kind of inversion method. Later versions of TOVS Export Package use more suitable cloud correction algorithms. The results from the ordinary inversion method, FXTIRO, are shown in Fig. 7.2, while the results from our method, THAP, are shown in Fig. 7.3.

We had to determine the regularization parameters λ_T and λ_V in THAP. A subjective estimation was done. Fifteen radiosonde launches were done from Onsala at the same time as the satellite passage. One radiosonde at the beginning of the period and one at the end of the period were selected. The nearest satellite sounding to each radiosonde was compared to the radiosonde, trying different values λ_T and λ_V. The couple $\lambda_T = 0.03$ and $\lambda_V = 0.06$ was subjectively estimated to give the best result. We use the same regularization parameters in the whole area and during the whole time period.

Our method shows a large RMS-difference around the tropopause. This is not unexpected, because there generally exists a sharp edge in the temperature profile at the tropopause. The penalty term, we have used for the temperature profile, will smooth the temperature around the tropopause too much. If we have some information about the tropopause we may use this in the spline approximation of temperature, by placing a knot with multiplicity three at the tropopause. This will give discontinuities in the first and second derivatives at the multiple knot, which we believe will give a better approximation of temperature around the tropopause. We first test our method of including tropopause information by using an accurate tropopause. Radiosondes were launched from Onsala, at the same time as the satellite passage. The first tropopause, according to the WMO definition, was calculated and a multiple knot was placed there. During the test period the tropopause were varying between 214 and 317 mb, for the thirteen used radiosonde launches. Such an accurate tropopause is not available for the whole area.

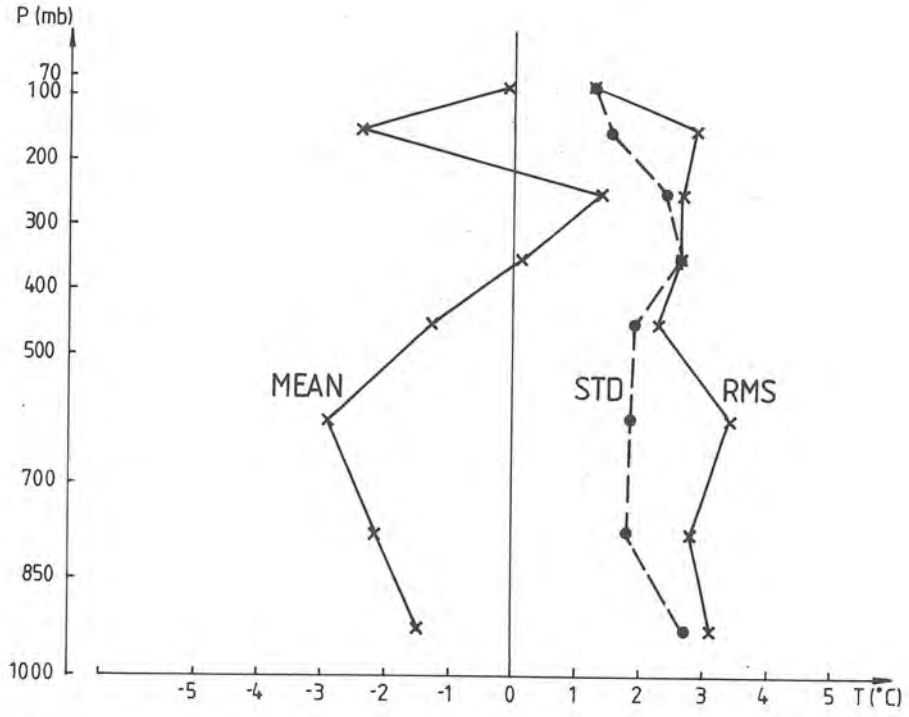

Figure 7.2 Differences in layer mean temperature between satellite soundings from FXTIRO and radiosondes, launched in the Meso-scale Analysis Area. 104 clear retrievals are included.

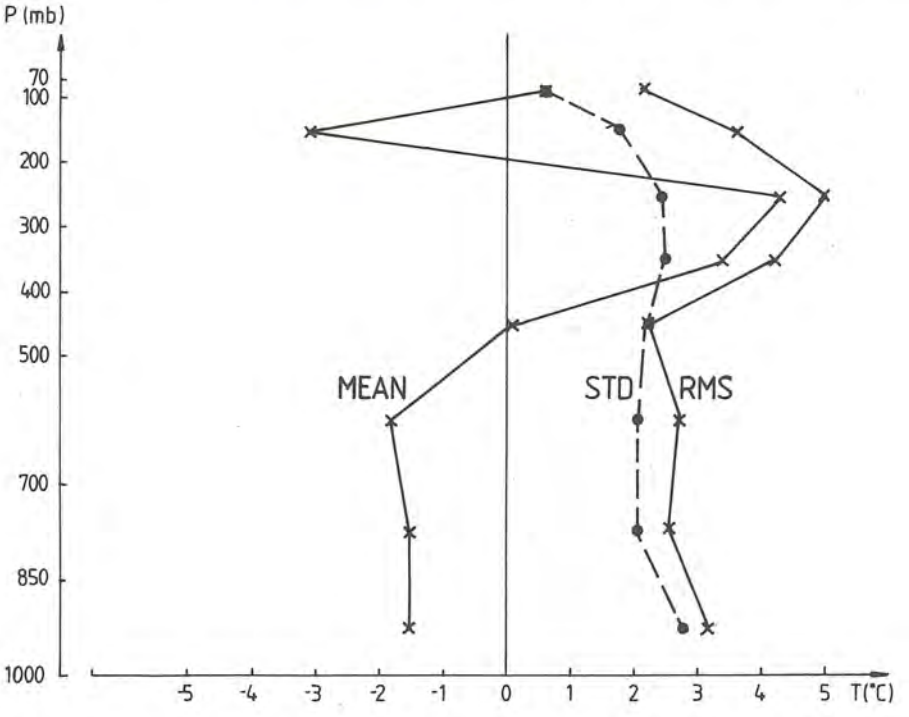

Figure 7.3 Differences in layer mean temperature between satellite soundings from THAP, without tropopause information, and radiosondes launched in the Meso-scale Analysis Area. 118 clear retrievals are included.

We checked the sensitivity of tropopause errors in the temperature retrieval, by adding and subtracting 50 mb to the tropopause, and used these new tropopauses in THAP, with λ_T = 0.05. The result is shown in Fig. 7.4. The same multiple knot was then used for the whole area with λ_T = 0.05. The results are shown in Fig. 7.5. We have significantly reduced the error around the tropopause. In Fig. 7.6 we demonstrate the influence of the incorporated tropopause on the temperature retrieval for one satellite sounding.

In an operational system, the tropopause information might be derived in different ways.

1) An objective analysis of the tropopause from the available, or a future sparser, radiosonde network will be done.

2) In the future a network of VHF radars, see Gage and Green (1982) might be used to give tropopause heights (and wind profiles).

3) In a well-balanced integrated system, the tropopause measurement should be done by a satellitebased instrument. Munteanu et al (1984) have proposed that tropopause height should be derived from TOMS Ozone Measurements.

One interesting issue is how the number of iterations in THAP, will influence the temperature retrieval. Once again we use the thirteen radiosondes, launched at Onsala, for the comparisons. The absolute values of the changes in layer mean temperatures, $\Delta T(P_1,P_2)$, in each iteration were calculated. The mean value of $|\Delta T(P_1,P_2)|$ for eight pressure layers were calculated from thirteen retrievals near Onsala.

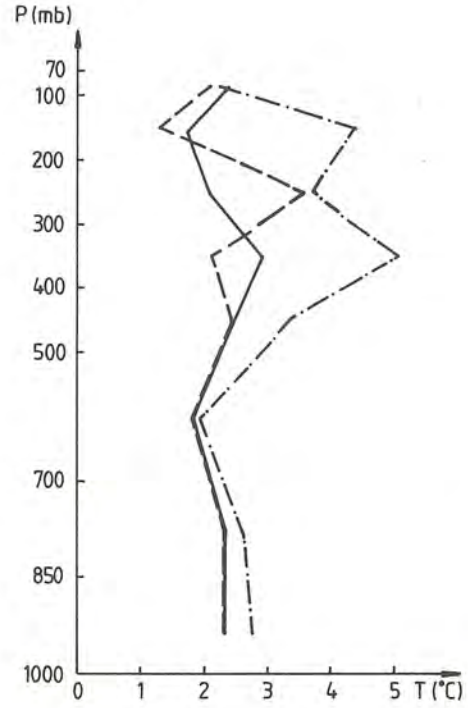

Figure 7.4 RMS differences in layer mean temperature between satellite soundings from THAP, with tropopauseinformation, and radiosondes launched from Onsala. The RMS differences are shown for three different tropopauses in THAP. The three cases are

——— = tropopause from radiosonde,
------ = tropopause from radiosonde + 50 mb,
—.—.— = tropopause from radiosonde - 50 mb.
Thirteen clear retrievals are included.

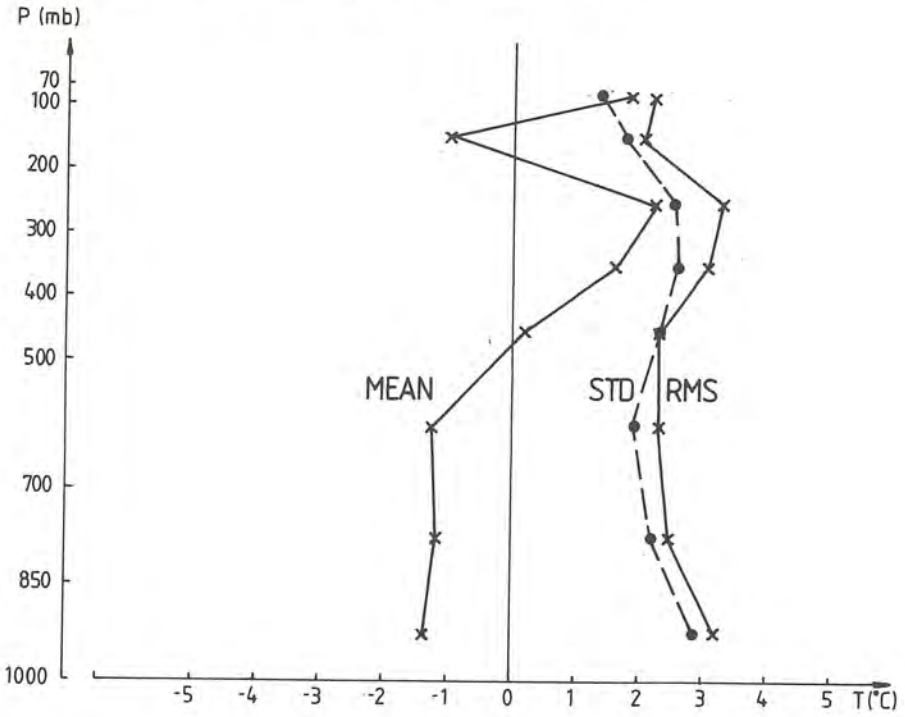

Figure 7.5 Differences in layer mean temperature between satellite soundings from THAP, with tropopause information, and radiosondes launched in the Meso-scale Analysis Area. 118 clear retrievals are included.

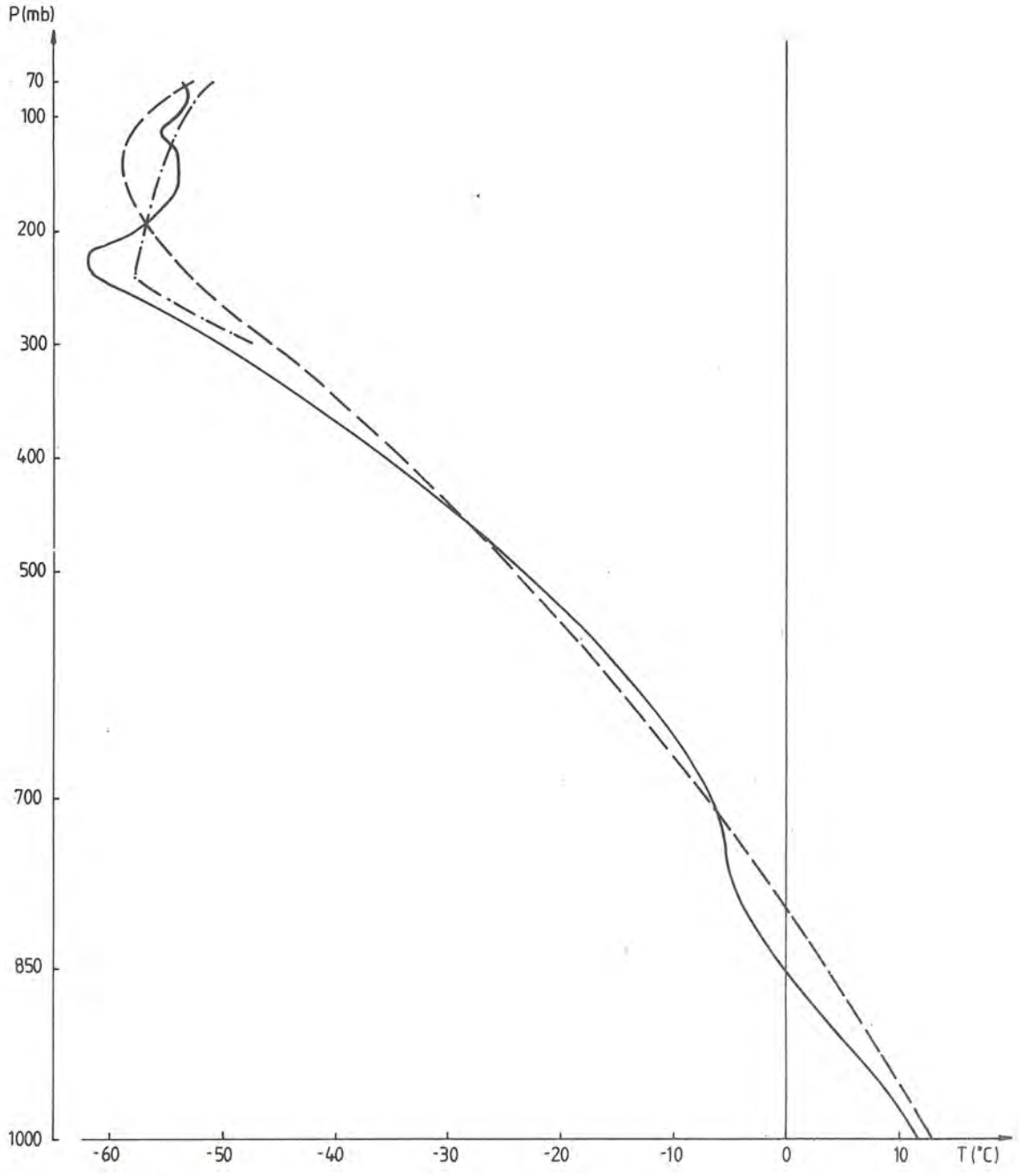

Figure 7.6 Temperature retrieval from one satellite sounding (1983-05-06 1345, 57°N, 12°E)

——— = radiosonde
------ = THAP, without tropopause
— . — = THAP, with tropopause
(temperature below 300 mb will coincide with the retrieval, without tropopause information)

Table 7.1 Absolute values of changes in layer mean temperatures, $|\Delta T(P_1,P_2)|$, for the first, second and third iteration in THAP. Mean values of thirteen clear retrievals near Onsala are calculated.

Pressure layer (P_1-P_2) mb	$\|\Delta T(P_1,P_2)\|$ 1 iteration ^oK	$\|\Delta T(P_1,P_2)\|$ 2 iterations ^oK	$\|\Delta T(P_1,P_2)\|$ 3 iterations ^oK
70- 100	1.78	0.26	0.04
100- 200	2.30	0.27	0.05
200- 300	2.78	0.51	0.08
300- 400	3.03	0.74	0.14
400- 500	3.39	0.80	0.13
500- 700	3.58	0.73	0.11
700- 850	2.33	0.51	0.07
850-1000	1.15	0.28	0.03

Table 7.1 shows a change of 2-3^{o}K in the first iteration, appr 0.5^{o}K in the second iteration and appr 0.1^{o}K in the third iteration. The second iteration will thus have a significant effect on the temperature retrieval. In Fig. 7.7 we compare the radiosonde retrievals with the retrievals from THAP with one and three iterations. The improvement, of the temperature retrievals between one and three iterations, is not quite clear. Errors in measurement variables, use of suboptimal regularization parameters and the fact that radiosondes do not give the 'true' temperature profiles are some of the factors, which make a comparison difficult.

The possible improvement of the result with several iterations must be compared with the extra computer time used for the iterations and for the more complex algorithms for selecting the regularization parameters.

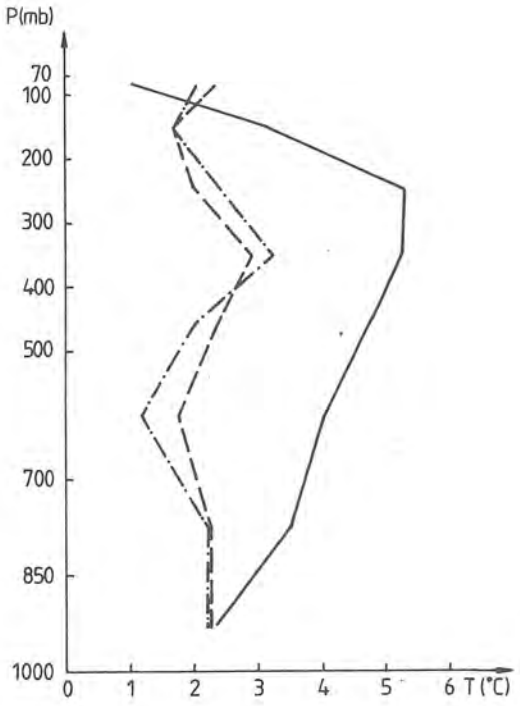

Figure 7.7 RMS differences in layer mean temperature between satellite soundings from THAP, with tropopauseinformation, and radiosondes launched from Onsala. The RMS differences are shown for different number of iterations in THAP

———— = initial guess

—.——. = 1 iteration

-------- = 3 iterations

Thirteen clear retrievals are included.

8. CONCLUSIONS

We have shown that the results from our inversion method THAP are comparable with the results from the ordinary retrieval method in the Physical Retrieval TOVS Export Package. With tropopause information included we will still have larger RMS differences in our method around the tropopause ($\approx 0.5^{o}K$) but smaller RMS differences between 500 and 850 mb ($0.5\text{-}1.0^{o}K$). Use of better regularization parameters (we used the same

in the whole area and in the whole time period) and a better approximation of tropopause height (we used the tropopause height measured at Onsala in the whole area) will likely improve our results. There is a lot of tuning to be done. The regularization parameters, the weights of the equations and the number and locations of the knots have to be decided. Some of these parameters might be changeable according to the area, the time of the season or the weather situation. In order to solve these problems, the next step will be to implement our inversion method in a quasi-operational TOVS processing system. The TOVS Export Package will form the base of the TOVS processing system.

Ancillary data, or ancillary information, could be included in the inversion method in three ways,

1) changing the locations and multiplicities of the knots,
2) adding equations,
3) adding linear equality and/or inequality constraints.

This will make our method capable of progress. The water vapour profiles might be improved and analysed. The use of some boundary layer model might be useful. The progress in TOVS retrievals done by the international community will be followed, and suitable algorithms will be implemented in our method. Cloud correction algorithms, using AVHRR-data, are believed to give a major improvement in the retrieval profiles.

We have in this paper calculated each temperature profile independent of the surrounding temperature retrievals. We have a one dimensional temperature retrieval method, working on each satellite sounding. An extension will be the three dimensional retrieval method. In a three dimensional method other atmospheric sensors, such as radiosondes, ground-based microwave radiometers and VHF-radars, could be included. A three dimensional method will also allow the inclusion of meteorological theory, e g in the form of simplified atmospheric equations of motion. This approach will require much more computer time, but seems promising. Three dimensional retrieval methods are described by Wahba and Wendelberger (1980) and Wahba (1984). Another future aspect is that the next generation of vertical profilers on TIROS-N will be launched in 1990. Microwave sensors will be used both for temperature and humidity profiling. This will reduce the cloud effects on the radiances, making the sounder an allweather instrument.

9. ACKNOWLEDGEMENTS

This work has been supported by the Swedish Space Corporation.

This work has required help from specialists in numerical analysis, atmospheric physics and meteorology. I will gratefully acknowledge the help I have received from Lars Eldén and Åke Björck (Linköping University), Jan Askne and Göran Skoog (Chalmers University of Technology) and Nils Gustafsson. Special thanks to Monika Johansson, who typed the manuscript, and Anita Bergstrand, who made the drawings.

10. REFERENCES

Aoki, T., 1982: An Improved Method to Retrieve the Clear Column Radiance from Partially Cloudy Spots of Radiometer on Board Satellite, Journal of The Meteorological Society of Japan, 60, 758-764.

Askne, J., 1984: Use of Ground-Based Microwave Radiometers for Nowcasting. Proceedings of the Second International Symposium on Nowcasting, Norrköping, Sweden, 3-7 September, 1984, 201-207.

Björck, Å. and L. Eldén, 1979: Methods in numerical algebra for ill-posed problems, Report LiTH-MAT-R-33-1979, Dept of Mathematics, Linköping University, 33 pp.

Chedin, A. and N.A. Scott, 1984: Improved Initialization Inversion Procedure. Technical Proceedings of The First International TOVS Study Conference, Igls, Austria, 29 August through 2 September, 1983, 14-79.

Craven, P. and G. Wahba, 1979: Smoothing Noisy Data with Spline Functions: Estimating the Correct Degree of Smoothing by the Method of Generalized Cross-Validation. Numerische Mathematik, 31, 377-403.

de Boor, C., 1978: A Practical Guide to Splines. Springer Verlag, New York.

Gage, K.S. and J.L. Green, 1982: An Objective Method for the Determination of Tropopause Height from VHF Radar Observations. Journal of Applied Meteorology, 21, 1150-1154.

Gill, P.E. and G.F. Miller, 1972: An algorithm for the integration of unequally spaced data. The Computer Journal, 15, 80-83.

Gill, P.E., W. Murray and M.H. Wright, 1981: Practical Optimization, Academic Press, London.

Golub, G.H., M. Heath and G. Wahba, 1979: Generalized Cross-Validation as a Method for Choosing a Good Ridge Parameter. Technometrics, 21, 215-223.

Golub, G.H. and C.F. van Loan, 1983: Matrix computations, The Johns Hopkins University Press, Baltimore, Maryland.

Gustafsson, N. and H. Törnevik, 1984: Development of an Operational System for Very-Short-Range Forecasting (VSRF) at SMHI. Proceedings of the Second International Symposium on Nowcasting, Norrköping, Sweden, 3-7 September, 1984, 473-477.

Hanson, R.J., 1971: A numerical method for solving Fredholm integral equations of the first kind using singular values, SIAM Journal of Numerical Analysis, 8, 616-622.

Hayden, C.M., W.L. Smith and H.M. Woolf, 1981: Determination of Moisture From NOAA Polar Orbiting Satellite Sounding Radiances, Journal of Applied Meteorology, 20, 450-466.

Hess, S.L., 1959: Introduction to theoretical meteorology, Henry Holt and Company, New York.

Holt, J.N. and D.L.B. Jupp, 1978: Free-knot Spline Inversion of a Fredholm Integral Equation from Astrophysics, J. Inst. Maths Applics, 21, 429-443.

Holton, J.R., 1979: An Introduction to Dynamic Meteorology, Academic Press, New York.

IMSL Library Reference Manual, Edition 8, 1980: International Mathematical and Statistical Library, Houston, Texas.

Lauritsen, L., G.J. Nelson and F.W. Porto, 1979: Data extraction and calibration of TIROS-N/NOAA radiometers. NOAA Technical Memorandum NESS 107. U.S. Department of Commerce, National Oceanic and Atmospheric Administration, National Earth Satellite Service, Washington D.C., 73 pp.

Liou, K-N., 1980: An Introduction to Atmospheric Radiation, Academic Press, New York.

McMillin, L.M., 1978: An Improved Technique for Obtaining Clear Radiances from Cloud-Contaminated Radiances. Monthly Weather Review, 106, 1590-1597.

McMillin, L.M. and C. Dean, 1982: Evaluation of a New Operational Technique for Producing Clear Radiances. Journal of Applied Meteorology, 21, 1005-1014.

Menzel, W.P. (editor), 1985: Technical Proceedings of The Second International TOVS Study Conference, Igls, Austria, 18-22 February, 1985, (to appear).

Munteanu, M.J., E.R. Westwater and N.C. Grody, 1984: Improvement of MSU Temperature Retrievals by Use of Tropopause Heights Derived from TOMS Ozone Measurements. Technical Proceedings of The First International TOVS Study Conference, Igls, Austria, 29 August through 2 September, 1983, 165-172.

NAG FORTRAN Library Manual, Mark 9, 1982: Numerical Algorithms Group, Oxford.

Oort, A.H. and E.M. Rasmusson, 1971: Atmospheric Circulation Statistics, NOAA Professional Paper 5, U.S. Department of Commerce, National Oceanic and Atmospheric Administration, 323 pp.

O'Sullivan, F. and G. Wahba, 1984: A cross validated bayesian retrieval algorithm for non-linear remote sensing experiments. Technical Report No 747, Dept of statistics, University of Wisconsin, Madison, Wisconsin, 20 pp.

Prata, A.J., 1985: Clear column radiances by optimal estimation. Technical Proceedings of The Second International TOVS Study Conference, Igls, Austria, 18-22 February, 1985, (to appear).

Smith, W.L., 1966: Note on the Relationship Between Total Precipitable Water and Surface Dew Point, Journal of Applied Meteorology, 5, 726-727.

Smith, W.L. and H.M. Woolf, 1976: The Use of Eigenvectors of Statistical Covariance Matrices for Interpreting Satellite Sounding Radiometer Observations. Journal of the Atmospheric Sciences, 33, 1127-1140.

Smith, W.L., 1983: Passive radiometry for vertical sounding from meteorological satellites, Applied Optics, 22, 2641-2643.

Smith, W.L., H.M. Woolf, C.M. Hayden, A.J. Schreiner and J.F. LeMarshall, 1984: The Physical Retrieval TOVS Export Package. Technical Proceedings of The First International TOVS Study Conference, Igls, Austria, 29 August through 2 September, 1983, 227-278.

Smith, W.L., H.M. Woolf, C.M. Hayden and A.J. Schreiner, 1985: The simultaneous retrieval export package. Technical Proceedings of The Second International TOVS Study Conference, Igls, Austria, 18-22 February, 1985, (to appear).

Stoer, J., 1971: On the numerical solution of constrained least-squares problems. SIAM Journal of Numerical Analysis, 8, 382-411.

Susskind, J. and M.T. Chahine, 1984: The GLAS Physical Numerical Algorithm for Analysis of HIRS 2/MSU Data. Technical Proceedings of The First International TOVS Study Conference, Igls, Austria, 29 August through 2 September, 1983, 285-299.

Svensson, J., 1984: Temperature profile retrievals from TIROS Operational Vertical Sounder during the ONSAM-experiment. R & D notes 33, SMHI, Norrköping, Sweden, 13 pp.

Twomey, S., 1977: Introduction to the mathematics of inversion in remote sensing and indirect measurements. Elsevier, New York.

Wahba, G. and J. Wendelberger, 1980: Some New Mathematical Methods for Variational Objective Analysis Using Splines and Cross Validation. Monthly Weather Review, 108, 1122-1143.

Wahba, G., 1982: Constrained regularization for ill posed linear operator equations, with applications in meteorology and medicine, in Statistical Decision Theory and Related Topics III, ed. J.O. Berger and S.S. Gupta, Academic Press, New York, 383-418.

Wahba, G., 1984: Variational methods for multidimensional inverse problems. Technical Report No 755, Dept of statistics, University of Wisconsin, Madison, Wisconsin, 23 pp.

Weinreb, M.P., H.E. Fleming, L.M. McMillin and A.C. Neundorffer, 1981: Transmittances for the TIROS Operational Vertical Sounder, NOAA Technical Report NESS 85, U.S. Department of Commerce, National Oceanic and Atmospheric Administration, National Earth Satellite Service, Washington D.C., 65 pp.

Werbowetzki, A. (Ed.), 1981: Atmospheric Sounding User's Guide. NOAA Technical Report NESS 83, U.S. Department of Commerce, National Oceanic and Atmospheric Administration, National Earth Satellite Service, Washington D.C., 82 pp.

Appendix A

LIST OF SYMBOLS AND NOTATIONS

A.1 Constants

Acceleration due to gravity at sea level	$g_o = 9.81\ m \cdot s^{-2}$
Gas constant for dry air	$R_d = 287\ J \cdot K^{-1} \cdot kg^{-1}$
Specific heat of dry air at constant pressure	$C_p = 1004\ J \cdot K^{-1} \cdot kg^{-1}$
Saturation vapour pressure at 0^oC (273^oK)	$e_o = 6.11\ mb$
Latent heat of condensation at 0^oC (273^oK)	$L_o = 2.5 \cdot 10^6 J \cdot kg^{-1}$
Molecular weight of water vapour divided by molecular weight of dry air	$\varepsilon = 0.622$

A.2 General notations for vectors and matrices and some useful definitions

Throughout this paper, we will indicate matrices with a double wavy underline and vectors with one wavy underline. The element in row 'i' and column 'j' for a matrix $\underset{\approx}{A}$ is denoted a_{ij} and the element 'i' in a vector $\underset{\sim}{A}$ is denoted a_i. The column 'i' in a matrix $\underset{\approx}{A}$ is denoted $\underset{\sim}{A}_i$.

A diagonal matrix $\underset{\approx}{D} = \text{diag}\ (d_{11}, d_{22}, \ldots, d_{nn})$ is a matrix, where $d_{ij} = 0,\ i \neq j$.

The inner product of two n-dimensional vectors $\underset{\sim}{X}$ and $\underset{\sim}{Y}$ is

$$\underset{\sim}{X}^T \underset{\sim}{Y} = \sum_{i=1}^{n} x_i \cdot y_i \quad .$$

The Euclidean norm of a n-dimensional vector $\underset{\sim}{X}$ is

$$||\underset{\sim}{X}||_2 = \left(\sum_{i=1}^{n} x_i^2\right)^{1/2} = (\underset{\sim}{X}^T \underset{\sim}{X})^{1/2} \quad .$$

An orthogonal matrix $\underset{\approx}{Q}$, is a square matrix where $\underset{\sim}{Q}_i^T \cdot \underset{\sim}{Q}_j = 0,\ i \neq j$, and $\underset{\sim}{Q}_i^T \underset{\sim}{Q}_i = 1$.

A symmetric matrix $\underset{\approx}{A}$ is positive definite if $\underset{\sim}{X}^T \underset{\approx}{A} \underset{\sim}{X} > 0$ for all nonzero vectors $\underset{\sim}{X}$.

The least-squares solution $\underset{\sim}{X}$ to a linear equation system $\underset{\approx}{A} \cdot \underset{\sim}{X} = \underset{\sim}{B}$ is; find $\underset{\sim}{X}$ which satisfies

$$\min_{\underset{\sim}{X}} ||\underset{\approx}{A} \cdot \underset{\sim}{X} - \underset{\sim}{B}||_2 \ .$$

In a weighted least-squares problem, we find $\underset{\sim}{X}$ which satisfies

$$\min_{\underset{\sim}{X}} ||\underset{\approx}{W} \cdot \underset{\approx}{A} \cdot \underset{\sim}{X} - \underset{\approx}{W} \cdot \underset{\sim}{B}||_2 \ ,$$

where $\underset{\approx}{W}$ usually is a diagonal matrix.

Appendix B

AN ANALYSIS OF THE RADIATIVE TRANSFER EQUATION BY SINGULAR VALUE DECOMPOSITION

The linear system, derived from the radiative transfer equation in Section 5, may be analysed by doing a singular value decomposition (SVD) of the matrix. The singular value decomposition is described by Golub and van Loan (1983). The SVD-theorem says:

Any m by n matrix $\underset{\approx}{A}$ can be factored into $\underset{\approx}{A} = \underset{\approx}{U}\,\underset{\approx}{\Sigma}\,\underset{\approx}{V}^T$, where $\underset{\approx}{U}$ is an m by m orthogonal matrix, $\underset{\approx}{V}$ is an n by n orthogonal matrix and $\underset{\approx}{\Sigma}$ is an m by n diagonal matrix where $\underset{\approx}{\Sigma} = \mathrm{diag}(\sigma_1,\sigma_2,\ldots,\sigma_{\min(m,n)})$. The singular values σ_i can be assumed to be ordered so that $\sigma_1 \geq \sigma_2 \geq \sigma_{\min(m,n)} \geq 0$, with 'r' singular values $\neq 0$.

In terms of the SVD the solution of the least-squares problem

$$\min_{\underset{\sim}{X}} ||\underset{\approx}{A}\cdot\underset{\sim}{X}-\underset{\sim}{B}||_2 \quad , \tag{B.1}$$

will be

$$\underset{\sim}{X} = \sum_{i=1}^{r} (\underset{\sim}{U}_i^T\cdot\underset{\sim}{B})/\sigma_i\cdot\underset{\sim}{V}_i \ . \tag{B.2}$$

If m<n then there is no unique solution $\underset{\sim}{X}$, (B.2) will give the solution $\underset{\sim}{X}$ with minimum Euclidean norm. We notice that $\underset{\sim}{X}$ is written as a linear combination of the vectors $\underset{\sim}{V}_i$. We assume that the error in $\underset{\sim}{B}$ is $\Delta\underset{\sim}{B}$, then the error in $\underset{\sim}{X}$ will be

$$\Delta\underset{\sim}{X} = \sum_{i=1}^{r} (\underset{\sim}{U}_i^T\cdot\Delta\underset{\sim}{B})/\sigma_i\cdot\underset{\sim}{V}_i \ . \tag{B.3}$$

We will show how SVD can be used to analyse the least-squares problem

$$\min_{\Delta\underset{\sim}{T},\Delta T_S} || \underset{\approx}{R}_T\cdot\Delta\underset{\sim}{T} + \underset{\sim}{R}_S\cdot\Delta T_S - \underset{\sim}{Y}||_2 \ , \tag{B.4}$$

which is (5.2) with the water vapour term neglected. This is also (B.1), with the notations

$$\underset{\approx}{A} = (\underset{\approx}{R}_T \; \underset{\sim}{R}_S) \;, \quad \underset{\sim}{X} = \begin{pmatrix} \Delta\underset{\sim}{T} \\ T_S \end{pmatrix} \;, \quad \underset{\sim}{B} = \underset{\sim}{Y} \;.$$

In ill-conditioned problems, like B.4, the singular values will tend to zero rapidly. If we solve (B.4) exactly, we will have a physically unacceptable solution. The measurement errors in $\underset{\sim}{Y}$ will be amplified for those terms in (B.3) corresponding to singular values much smaller than one.

We will use ten HIRS-channels (channel 3,4,5,6,7,8,13,14,15 and 16) and two MSU-channels (channel 3 and 4) in the SVD of (B.4). The SVD is calculated with subroutine LSVDF in the IMSL software library.
The temperature profile is between the pressure levels 10 and 1000 mb, and is discretized into 30 levels. The matrix in (B.4) is calculated in the same way as described in Section 5. Each row, corresponding to channel ν, has been multiplied with $1/\frac{\partial B_\nu(B^{-1}(I_\nu)}{\partial T}$. We have done a SVD for twelve climates, taken from Oort and Rasmusson (1971). These are winter, spring, summer and autumn for latitudes 35^oN, 55^oN and 75^oN. In Table B.1, we show the eight largest singular values for each climate (the smallest singular values for each climate are in the interval 0.0001-0.0005). We also show the corresponding vectors $\underset{\sim}{V}_1,\ldots,\underset{\sim}{V}_8$ and $\underset{\sim}{U}_1,\ldots,\underset{\sim}{U}_8$ for the climate in spring, 55^oN in Fig. B.1 and B.2 respectively. The vectors $\underset{\sim}{V}_i$ show the ability of the TOVS instrument to discover temperature differences from the initial guess at different levels. The vectors $\underset{\sim}{U}_i$ show the relative importance each channel has on the i:th term in (B.2). The singular values are sorted in decreasing order, then the measurement error is expected to influence more and more for each new term added in (B.2). Note that $||\underset{\sim}{U}_i||_2 = ||\underset{\sim}{V}_i||_2 = 1$ and the elements in $\Delta\underset{\sim}{B}$, that is the errors in brightness temperatures, are approximately one. We note that in none of the five vectors $\underset{\sim}{V}_1,\ldots,\underset{\sim}{V}_5$, there is a major contribution from the lower atmosphere (>850 mb).

We calculate (B.2) for one real satellite sounding near to Onsala in May, 1983. The initial guess, $T^{(0)}$ and $T_S^{(0)}$, is climate in spring, 55^oN. We calculate (B.2) with 1, 3, 5 and 7 terms. This is the method of truncated singular value decomposition, described by Hanson (1971). The retrieved temperatures, $\underset{\sim}{T} = \underset{\sim}{T}^{(0)} + \Delta\underset{\sim}{T}$ and $T_S + \Delta T_S$, were compared with radiosonde measurements done at Onsala at the same time, and are

Table B.1 The eight largest singular values of the matrix in (B.4) for different climates

Season	35°N	55°N	75°N
Winter	1.15,0.51,0.32,0.20, 0.07,0.06,0.02,0.006	1.29,0.52,0.29,0.18, 0.06,0.05,0.01,0.008	1.31,0.51,0.30,0.18, 0.06,0.05,0.01,0.008
Spring	1.09,0.51,0.33,0.20, 0.08,0.06,0.03,0.007	1.24,0.52,0.29,0.18, 0.06,0.05,0.01,0.008	1.28,0.54,0.28,0.17, 0.06,0.05,0.01,0.006
Summer	0.90,0.53,0.34,0.21, 0.08,0.06,0.03,0.011	1.06,0.53,0.31,0.19, 0.06,0.05,0.02,0.008	1.17,0.54,0.29,0.18, 0.06,0.05,0.01,0.010
Autumn	1.00,0.52,0.34,0.21, 0.08,0.06,0.03,0.009	1.20,0.52,0.30,0.19, 0.06,0.05,0.02,0.008	1.27,0.53,0.29,0.18, 0.06,0.05,0.01,0.008

shown in Fig. B.3. When using one term, only the surface skin temperature is changed. The vector $\underset{\sim}{V}_1$ gives a major contribution to the surface skin temperature but will not change the atmospheric temperature. The vector $\underset{\sim}{U}_1$ shows that the most important channel in the calculation of the first term is HIRS 8, which is a window channel. These, not unexpected, results is an example of how the vectors $\underset{\sim}{V}_i$ and $\underset{\sim}{U}_i$ can be interpretated. With three and five terms the temperature retreivals are improved. There is still no significant change in the lower atmosphere. When seven terms were used, there is a change in the lower atmosphere, but now the influence of measurement errors is noticeable. We find these oscillations, in the temperature profile, which is typical for ill-conditioned problems (if we use eight terms, we will have T(1000) = 73.1°C and T(700) = -136.5°C).

We have shown, that satellite measurements alone cannot give enough information about the temperature profile. We may improve the temperature retrieval by doing independent measurements of relevant variables, such as surface temperature, and use information about the behaviour of the atmospheric temperature profile. We have also shown the potential of singular value decomposition, when analysing linear systems in remote sensing of temperature profiles.

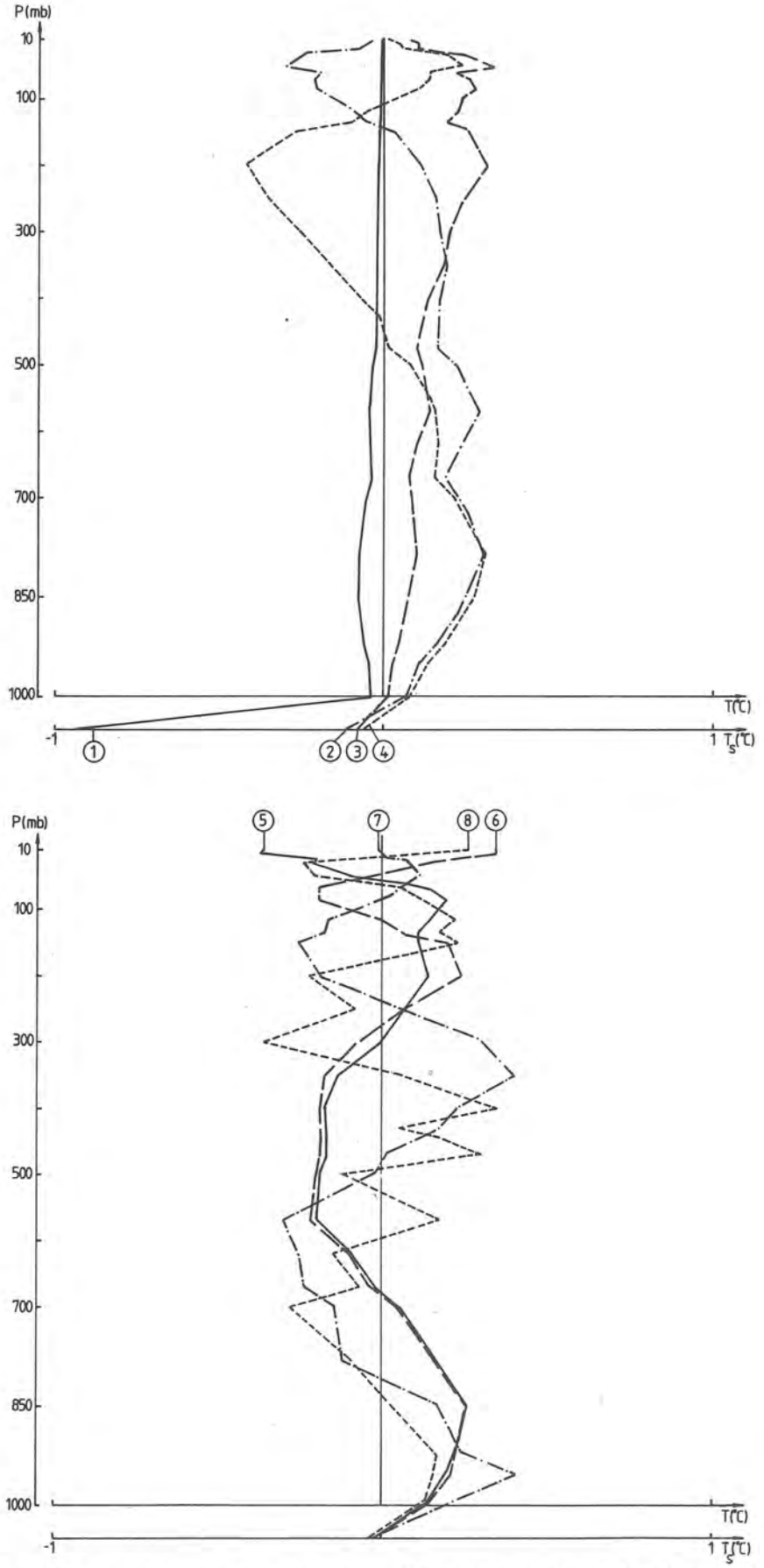

Figure B.1 Left singular vectors $\underset{\sim}{V}_1,\ldots,\underset{\sim}{V}_8$ of $(\underset{\approx}{R}_T\ \underset{\sim}{R}_S)$ calculated for the climate in spring, 55^{o}N.

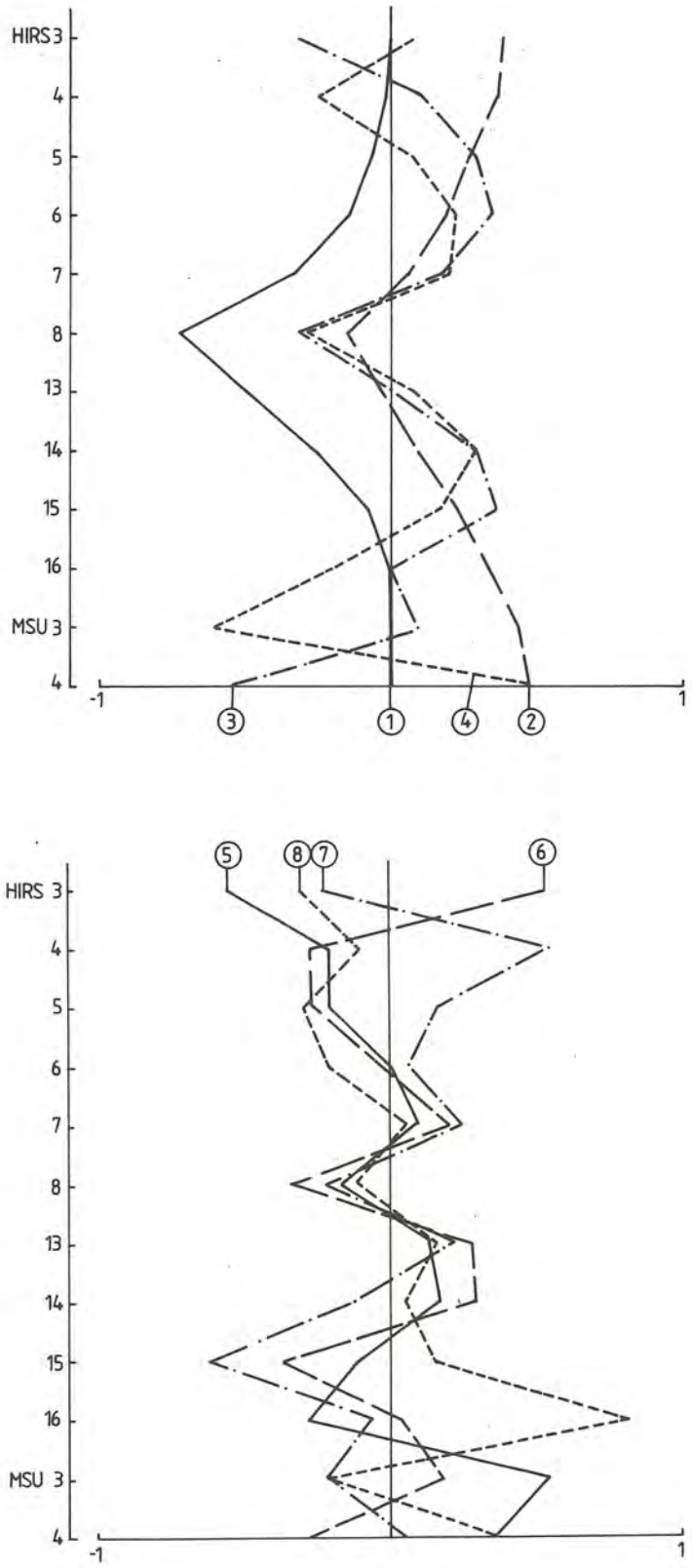

Figure B.2 Right singular vectors $\underset{\sim}{U}_1,\ldots,\underset{\sim}{U}_8$ of $(\underset{\approx}{R}_T\ \underset{\sim}{R}_S)$ calculated for the climate in spring, 55^{o}N.

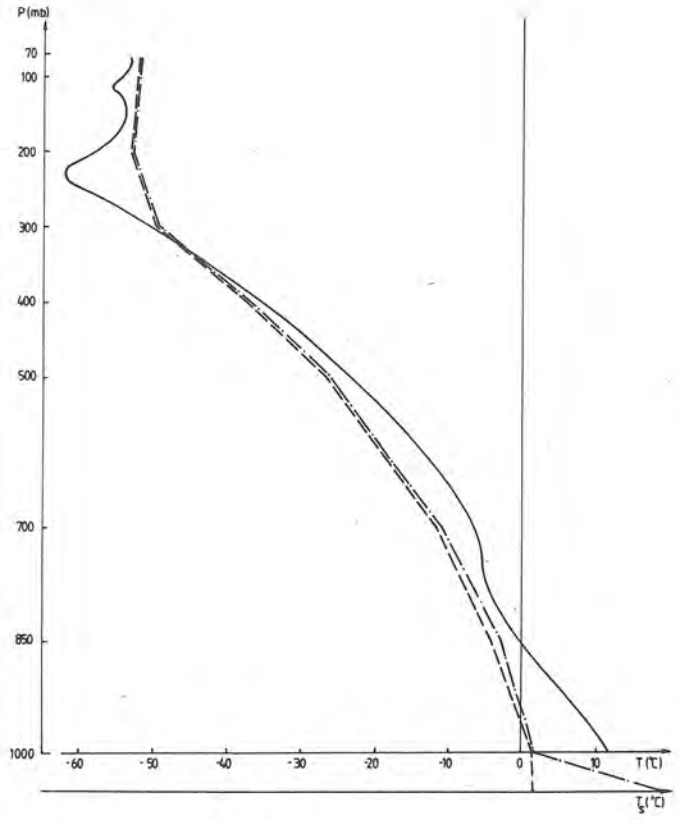

1 term

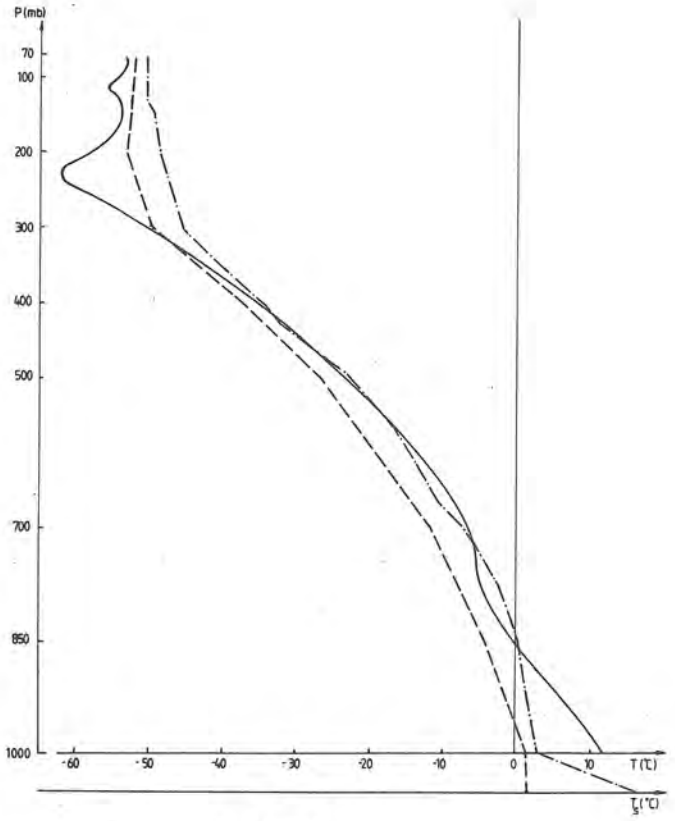

3 terms

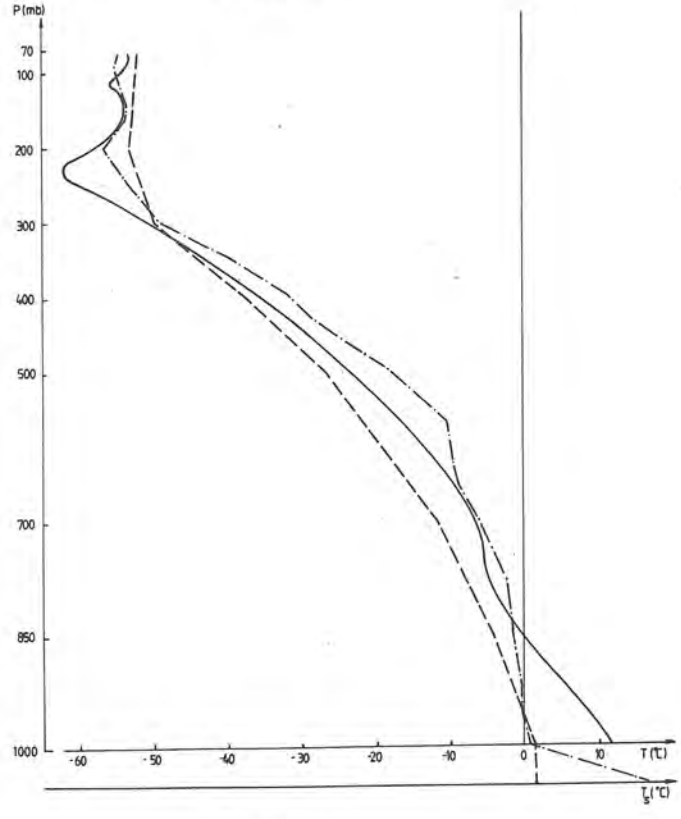

5 terms

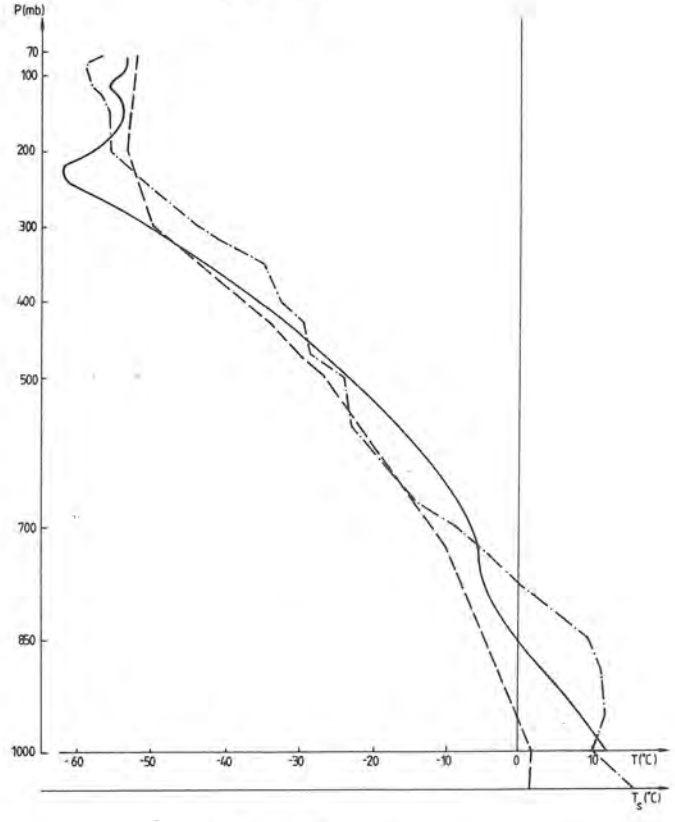

7 terms

Figure B.3 Truncated SVD of (B.4) with 1, 3, 5 and 7 terms

———— radiosonde

--------- initial guess

—.—.—.—.— temperature retrieval from truncated SVD

Appendix C

CALCULATION OF THE LINEAR EQUATION SYSTEM FROM THE TAYLOR EXPANSION OF THE RADIATIVE TRANSFER EQUATION

We will show how the numerical calculation of $\underset{\sim}{Y}$, $\underset{\approx}{R}_T$, $\underset{\sim}{R}_S$ and $\underset{\approx}{R}_V$ in (5.2) can be done. The variables T, V and P are discretized into 'n' levels. We do not allow the temperature to be changed above level 11 (= 10 mb) and we do not allow the water vapour mixing ratio to be changed above level 26 (= 300 mb).

We have to calculate $\frac{\partial \tau_\nu}{\partial P}$ for different pressure levels. This has to be done with some numerical differentation method. We have

$$\frac{\partial \tau_\nu(p_1)}{\partial P} = (\tau_\nu(p_2) - 1)/p_2 \quad ,$$

$$\frac{\partial \tau_\nu(p_j)}{\partial P} = (\tau_\nu(p_{j+1}) - \tau_\nu(p_{j-1}))/(p_{j+1}-p_{j-1}) \quad , \qquad j = 2,3,\ldots,n-1$$

$$\frac{\partial \tau_\nu(p_n)}{\partial P} = (\tau_\nu(p_n) - \tau_\nu(p_{n-1}))/(p_n-p_{n-1}) \qquad \text{(C.1)}$$

The elements y_ν are from (5.1), which says (we repeat)

$$y_\nu = \tilde{I}_\nu - \varepsilon_\nu \cdot B_\nu(T_S^{(0)}) \cdot \tau_\nu(P_S) + \int_0^{P_S} B_\nu(T^{(0)}) \frac{\partial \tau_\nu(P)}{\partial P} dP.$$

The integral in (5.1) must be calculated using some numerical quadrature method. We use the method by Gill and Miller (1972), which is suitable for integration of unequally spaced data.

The radiance is affected by the temperature in two ways; the Planck function and the transmittance dependency of the temperature. The transmittance dependency of temperature is weak, so in the calculation of $\frac{\partial I_\nu^{(0)}}{\partial \tilde{I}}$ we neglect this dependency. By using the numerical differentation scheme in (C.1) and the trapezoidal rule for the integral calculation, we have

$$\frac{\partial I_\nu^{(0)}}{\partial t_j} = 0 \quad , \qquad j = 1,\ldots,10$$

$$\frac{\partial I_\nu^{(0)}}{\partial t_j} = (\tau_\nu(p_{j-1}) - \tau_\nu(p_{j+1})) \cdot \frac{dB(t_j^{(0)})}{dT} \cdot 0.5, \qquad j = 11,\ldots,n-1$$

$$\frac{\partial I_\nu^{(0)}}{\partial t_n} = (\tau_\nu(p_{n-1}) - \tau_\nu(p_n)) \cdot \frac{dB(t_n^{(0)})}{dT} \cdot 0.5 \qquad \text{(C.2)}$$

The calculation of $\frac{\partial I_\nu^{(0)}}{\partial T_S}$ gives

$$\frac{\partial I_\nu^{(0)}}{\partial T_S} = \varepsilon_\nu \cdot \frac{dB(T_S^{(0)})}{dT} \cdot \tau_\nu(P_S) \quad . \qquad \text{(C.3)}$$

If the water vapour mixing ratio W is changed, then radiance will be changed, because the transmittance depends on W. The transmittance is more or less sensitive, for changes in W, for different channels. The most sensitive channels are those, which are best suited for determination of water vapour mixing ratio. We use the same HIRS-channels, as in the calculation of $\frac{\partial I_\nu}{\partial T}$. We may in an operational system, without loss of accuracy use only a few channels (e.g. HIRS channels 10, 11, 12 and some window channels).

The variable W is input parameter in the subroutines for transmittance calculations. It is convenient to calculate $\frac{\partial I_\nu}{\partial v_j} = \frac{\partial I_\nu}{\partial w_j} \cdot \frac{\partial w_j}{\partial v_j} = \frac{\partial I_\nu}{\partial w_j} \cdot w_j$.

We have to use some numerical differentation method in the calculation of $\frac{\partial I_\nu^{(0)}}{\partial w_j}$. We make a forward-difference approximation, which gives

$$\frac{\partial I_\nu^{(0)}}{\partial w_j} = (\varepsilon_\nu \cdot B_\nu(T_S^{(0)}) \cdot (\tau_\nu(P_S, W^{(0)}+\Delta W_j) - \tau_\nu(P_S, W^{(0)})) \cdot$$

$$- \int_0^{P_S} B_\nu(T^{(0)}) \cdot \left(\frac{\partial \tau_\nu(P, W^{(0)}+\Delta W_j)}{\partial P} - \frac{\partial \tau_\nu(P, W^{(0)})}{\partial P}\right) \cdot dP) / \Delta W_j * w_j^{(0)} \ ,$$

$$j = 26,27,..,n \qquad \text{(C.4)}$$

where

$$\Delta W_j(P) = \begin{cases} 0 & , \quad P \leq p_{j-1} \\ \Delta w_j \cdot (P-p_{j-1})/(p_j-p_{j-1}) & , \quad p_{j-1} < P \leq p_j \\ \Delta w_j \cdot (p_{j+1}-P)/(p_{j+1}-p_j) & , \quad p_j < P \leq p_{j+1} \\ 0 & , \quad P > p_{j+1} \end{cases}$$

and we explicitly declare the transmittance dependency of W by the notation $\tau(P,W)$. The numerical differentiation scheme in (C.1) and the trapezoidal rule will be used in the calculation of (C.4).

The calculation of $\frac{\partial I_\nu}{\partial \underset{\sim}{V}}$ is very time-consuming, that is because it involves a great number of transmittance calculations. An effective calculation of $\frac{\partial I_\nu}{\partial \underset{\sim}{V}}$ will give a considerable reduction of the total computational time of the inversion method. We may decrease the computation time by using our knowledge that, in the software package, τ is calculated as a product of four transmittances,

$$\tau(P,W,T,\rho) = \text{O3TAU}(P) \cdot \text{CO2TAU}(P) \cdot \text{H2OTAU}(P) \cdot \text{CONTAU}(P) \ ,$$

where O3TAU depends on total ozone amount above P, CO2TAU depends on temperature above P. H2OTAU depends on the integrated amount of water vapour above P and CONTAU depends on water vapour at P. The notations O3TAU, CO2TAU, H2OTAU and CONTAU are the names of the subroutines for transmittance calculations.

Appendix D

SENSITIVITY ANALYSIS OF THE RADIATIVE TRANSFER EQUATION

Several types of errors influence the calculation of $\underset{\sim}{Y}$ in 5.2. These are errors depending on

1) cloud contamination,
2) surface emissivity,
3) surface pressure approximation,
4) transmittance calculation and sensors,
5) water vapour approximation,
6) temperature approximation over a specified layer,
7) ozone,
8) numerical quadrature.

These errors are, more or less, influencing the observed and calculated radiances. They are in some cases wellknown, in other cases not. A survey of the errors are given below.

The radiative transfer equation is described in Section 3. We make a slight modification of (3.1), and receive

$$I_\nu = \varepsilon_\nu \cdot B_\nu(T_S) \cdot \tau_\nu(P_S,T,W,\rho) - \int_0^{P_S} B_\nu(T) \cdot \frac{\partial \tau_\nu(P,T,W,\rho)}{\partial P} \cdot dP \ , \qquad (D.1)$$

In (D.1) we have explicitly noted that transmittance depends on temperature (T), water vapour (W) and ozone content (ρ) between the pressure level of interest and the satellite.

Cloud contamination

Several methods exist for correction of cloud contamination of infrared channels. In Aoki (1982) the RMS errors of radiances in percent are given for different methods. The following approximative RMS errors are valid for Aoki's QA-method using AVHRR-data

HIRS Channel	1	2	3	4	5	6	7	8	9	10	11	12	13	14	15	16	17	18	19
Error %	0	0	0	1	1	1	1	0	1	1	1	1	3	3	3	1	0	5	5

One should notice that this error estimation probably is too optimistic over land, because Aoki's method is only used over oceans. Cloud contamination errors are neglected for MSU-channels.

The technique to use AVHRR-data in the correction of cloud-contaminated radiances is very promising. However, it requires a lot of computer time. Algorithms, not using AVHRR-data, are presented in McMillin (1978), McMillin and Dean (1982) and Prata (1985).

Surface emissivity

An error $\Delta\varepsilon_\nu$ is assumed in emissivity ε_ν for each channel ν. Error ΔI_ν in radiance will be

$$\Delta I_\nu = \Delta\varepsilon_\nu \cdot B_\nu(T_S) \cdot \tau_\nu(P_S,T,W,\rho) \ .$$

Surface pressure

An error ΔP_S is assumed in surface pressure P_S.

$$\Delta I_\nu = \varepsilon_\nu \cdot B_\nu(T_S) \cdot (\tau_\nu(P_S+\Delta P_S,T,W,\rho) - \tau_\nu(P_S,T,W,\rho)) - \int_{P_S}^{P_S+\Delta P_S} B_\nu(T) \frac{\partial \tau_\nu(P,T,W,\rho)}{\partial P} \cdot dP \ .$$

Transmittance calculation and sensors

Errors in sensors and in the calculation of transmittance τ, make it necessary to do empirical adjustments of τ. One of the most common adjustments is the gamma-delta procedure. In Susskind and Chahine (1984) the errors in brightness temperature, after gamma-delta correction, are estimated to 0.7^oK. This error may include some of the other errors, e g uncertainties in surface emissivity, but is a fairly good approximation of the error depending of transmittance calculation and sensors.

Water vapour approximation

Water vapour cannot be determined exactly. This will change the transmittance of radiances. An error ΔW is assumed in water vapour W.

$$\Delta I_\nu = \varepsilon_\nu \cdot B_\nu(T_S) \cdot (\tau_\nu(P_S,T,W+\Delta W,\rho) - \tau_\nu(P_S,T,W,\rho))$$
$$- \int_0^{P_S} B_\nu(T) \cdot \left(\frac{\partial \tau_\nu(P,T,W+\Delta W,\rho)}{\partial P} - \frac{\partial \tau_\nu(P,T,W,\rho)}{\partial P}\right) \cdot dP \ .$$

Temperature approximation above a specified layer

For meteorological purposes we are not interested in calculating temperature for the highest levels (highest level is 0.1 mb). An approximation, e g climate, of the temperature profile above a certain pressure level P_ℓ is done. Assuming that the error in this approximation is ΔT the error in radiance will be

$$\Delta I_\nu = -\int_0^{P_\ell} (B_\nu(T+\Delta T) - B_\nu(T)) \frac{\partial \tau_\nu(P,T,W,\rho)}{\partial P} \cdot dP \ .$$

Ozone

Ozone in the atmosphere affects the transmittance. While ozone amount in atmosphere is not known exactly, an error will be introduced. An error $\Delta\rho$ is assumed for ozone amount ρ.

$$\Delta I_\nu = \varepsilon_\nu \cdot B_\nu(T_S) \cdot (\tau_\nu(P_S,T,W,\rho+\Delta\rho) - \tau_\nu(P_S,T,W,\rho))$$
$$- \int_0^{P_S} B_\nu(T) \cdot \left(\frac{\partial \tau_\nu(P,T,W,\rho+\Delta\rho)}{\partial P} - \frac{\partial \tau_\nu(P,T,W,\rho)}{\partial P}\right) \cdot dP$$

For MSU-channels and for HIRS-channels 8, 10-19 the influence of ozone is neglected. HIRS-channel 9 is used for ozone calculation.

Numerical quadrature

The calculation of the integral in the radiative transfer equation requires a numerical quadrature method. This will introduce an error,

which should be estimated. An error estimation is often included in subroutines from the numerical software libraries.

In order to see how different errors are influencing the radiances, a simple interactive program was constructed. The user may vary the estimation of different errors. A table with the individual errors is printed. Different temperature and water vapour profiles are used. These are winter, spring, summer and autumn climate from 35^{o}, 55^{o} and 75^{o}N. The climate is from Oort and Rasmusson (1971). The integral is calculated with the method of Gill and Miller (1972). Radiance errors are transformed to brightness temperatures, by doing a multiplication with $1/\frac{\partial B_{\nu}(B^{-1}(I_{\nu}))}{\partial T}$. In Table D.1 the result for the climate in spring, 55^{o}N is presented.

We have suggested a method for error analysis of RTE. This method could be refined. The two largest errors, 'cloud contamination' and 'transmittance calculation and sensors', are those which are most uncertain. From Table D.1, we suggest a total error in brightness temperature of 1^{o}K. This is a conservative suggestion. Susskind and Chahine (1984) and Chedin and Scott (1984) contain dicussions about the radiance errors.

Table D.1 Errors in brightness temperature; ^{o}K.
Temperature and humidity from climate in spring, $55^{o}N$. We use the RMS errors from Aoki's QA-method in the estimation of errors from correction of cloud contamination.

Emissivity ε for HIRS-channels are from Chedin and Scott (1984) (over land) see Table 6.1. Emissivity for all MSU-channels = 0.95, $\Delta\varepsilon$ = 0.01 for all channels.
Surface pressure P_S = 1000 mb, ΔP_S = 10 mb.
Transmittance calculation and sensors: Error $\approx 0.7^{o}K$.
Error in water vapour (g/Kg) = 10%.
Error in temperature (above 10 mb) = $1^{o}K$.
Ozone ρ = 347 Dobson Units, $\Delta\rho$ = 25 Dobson Units.

ERRORS RELATED TO

		NUMERICAL QUADRATURE	CLOUD CONTAMINATION	EMISSIVITY	SURFACE PRESSURE	TRANSMITTANCE CALCULATION AND SENSORS	WATER VAPOUR	TEMPERATURE	OZONE
HIRS	1	1.19	.00	.00	.00	.70	.00	.45	.00
	2	.10	.00	.00	.00	.70	.00	.16	.01
	3	.07	.00	.00	.00	.70	.00	.12	.00
	4	.06	.51	.00	.02	.70	.01	.06	.02
	5	.09	.55	.05	.18	.70	.04	.06	.08
	6	.09	.57	.12	.34	.70	.09	.03	.08
	7	.08	.61	.29	.43	.70	.19	.02	.06
	8	.01	.00	.55	.13	.70	.14	.00	.00
	9	.00	.50	.52	.00	.70	.00	.00	.00
	10	.02	.41	.34	.20	.70	.17	.00	.00
	11	.04	.32	.03	.19	.70	.55	.00	.00
	12	.06	.26	.00	.01	.70	.66	.00	.00
	13	.02	.66	.16	.14	.70	.04	.00	.00
	14	.02	.60	.08	.16	.70	.02	.01	.00
	15	.01	.53	.02	.08	.70	.01	.06	.00
	16	.10	.16	.00	.00	.70	.00	.15	.00
	17	.43	.00	.00	.00	.70	.00	.74	.00
	18	.00	1.01	.22	.03	.70	.01	.00	.00
	19	.00	.96	.21	.03	.70	.04	.00	.00
MSU	1	.06	.00	*	.04	.70	.01	.00	.00
	2	.03	.00	.28	.03	.70	.00	.00	.00
	3	.14	.00	.00	.00	.70	.00	.00	.00
	4	.09	.00	.00	.00	.70	.00	.01	.00

* MSU channel 1 is used for calculation of surface emissivity for microwave channels.

Appendix E

THE INVERSION METHOD WITH THREE ITERATIONS

In Section 5, we describe how we, from the initial guess $T^{(0)}$, $T_S^{(0)}$ and $V^{(0)}$, with our inversion method THAP get a better approximation $T^{(1)} = T^{(0)} + \Delta T$, $T_S^{(1)} = T_S^{(0)} + \Delta T_S$ and $V^{(1)} = V^{(0)} + \Delta V$. We mentioned that this process could be repeated with $T^{(1)}$, $T_S^{(1)}$ and $V^{(1)}$ as our new initial guess. In this Appendix we will show the algorithms in THAP with three iterations (k = 0,1,2). The notations are the same as in Section 5, but we note with an upper index '(k)', that this vector (or matrix) depends on $T^{(k)}$, $T_S^{(k)}$ and/or $V^{(k)}$, and have to be recalculated each iteration.

Step 1) Initial guess choosen.
Calculate the number of levels 'n' from surface pressure.

$$T^{(0)}(P) = \sum_{i=1}^{12} c_i^{(0)} \cdot B_i(\Psi_T, P) ,$$

$$V^{(0)}(P) = \sum_{i=1}^{9} d_i^{(0)} \cdot B_i(\Psi_V, P) ,$$

$$T_S^{(0)} = t_n(P_S) ,$$

$$k = 0 ,$$

$\underset{\approx}{S}$, $\underset{\approx}{U}$, $\underset{\approx}{L}_T$ and $\underset{\approx}{L}_V$ are calculated.

Step 2) Radiative transfer equation included.

$$\underset{\sim}{Y}^{(k)} = \underset{\approx}{R}_T^{(k)} \cdot \underset{\sim}{\Delta T}^{(k)} + \underset{\sim}{R}_S^{(k)} \cdot \Delta T_S^{(k)} + \underset{\approx}{R}_V^{(k)} \cdot \underset{\sim}{\Delta V}^{(k)} .$$

Step 3) Ancillary data included.

$$\Delta t_n^{(k)} = T_{OBS} - t_n^{(k)} ,$$

$$\Delta v_n^{(k)} = V_{OBS} - v_n^{(k)} ,$$

$$\Delta t_{11}^{(k)} = t_{11}^{(0)} - t_{11}^{(k)} ,$$

$$\Delta t_n^{(k)} - \Delta T_S^{(k)} = T_S^{(k)} - t_n^{(k)} ,$$

or

$$\underset{\approx}{A}_T \cdot \Delta \underset{\sim}{T}^{(k)} + \underset{\sim}{A}_S \cdot \Delta T_S^{(k)} + \underset{\approx}{A}_V \cdot \Delta \underset{\sim}{V}^{(k)} = \underset{\sim}{Z}^{(k)} .$$

Step 4) Linear least-squares problem defined.
Calculate the matrices in the linear least-squares problem

$$\min_{\underset{\sim}{F}^{(k)}} ||\underset{\approx}{K}^{(k)} \cdot \underset{\sim}{F}^{(k)} - \underset{\sim}{G}^{(k)}||_2^2 ,$$

where

$$\underset{\approx}{K}^{(k)} = \underset{\approx}{E} \cdot \begin{pmatrix} \underset{\approx}{R}_T^{(k)} \cdot \underset{\approx}{S} & \underset{\sim}{R}_S^{(k)} & \underset{\approx}{R}_V^{(k)} \cdot \underset{\approx}{U} \\ \underset{\approx}{A}_T & \underset{\sim}{A}_S & \underset{\approx}{A}_V \end{pmatrix} ,$$

$$\underset{\sim}{F}^{(k)} = \begin{pmatrix} \Delta \underset{\sim}{C}^{(k)} \\ \Delta T_S^{(k)} \\ \Delta \underset{\sim}{D}^{(k)} \end{pmatrix} ,$$

$$\underset{\sim}{G}^{(k)} = \underset{\approx}{E} \cdot \begin{pmatrix} \underset{\sim}{Y}^{(k)} \\ \underset{\sim}{Z}^{(k)} \end{pmatrix} .$$

Step 5) Linear constraints included.

$$\sum_{i=1}^{12} (B_i'(\Psi_T, p_j) - R_d/C_p \cdot B_i(\Psi_T, p_j)) \cdot \Delta c_i^{(k)} \leq$$

$$\sum_{i=1}^{12} (-B_i'(\Psi_T, p_j) + R_d/C_p \cdot B_i(\Psi_T, p_j)) \cdot c_i^{(k)} , \qquad j = 26, \ldots, n,$$

$$\sum_{i=1}^{9} B_i(\Psi_V, p_j) \cdot \Delta d_i^{(k)} - \beta/(t_j^{(k)} \cdot t_j^{(k)}) \cdot \sum_{i=1}^{12} B_i(\Psi_T, p_j) \cdot \Delta c_i^{(k)} \leq$$

$$\ln(\alpha/p_j) + \beta/(1/273 - 1/t_j^{(k)}) - v_j^{(k)} , \qquad j = 26, \ldots, n.$$

Step 6) Solve the linear least-squares problem with penalty terms and linear constraints.

$$\min_{\underset{\sim}{F}^{(k)}} \{ ||\underset{\approx}{K}^{(k)} \cdot \underset{\sim}{F}^{(k)} - \underset{\sim}{G}^{(k)}||_2^2 + \lambda_T ||\underset{\approx}{L}_T \cdot \Delta\underset{\sim}{C}^{(k)} + \underset{\approx}{L}_T \cdot \underset{\sim}{C}^{(k)}||_2^2 + \lambda_V ||\underset{\approx}{L}_V \cdot \Delta\underset{\sim}{D}^{(k)} + \underset{\approx}{L}_V \cdot \underset{\sim}{D}^{(k)}||_2^2 \} .$$

The problem is solved with Stoer's method.

Step 7) Calculate $T^{(k+1)}$, $T_S^{(k+1)}$ and $V^{(k+1)}$.

$$c_j^{(k+1)} = c_j^{(k)} + \Delta c_j^{(k)} \quad , \quad j = 1,2,\ldots,12 ,$$

$$d_j^{(k+1)} = d_j^{(k)} + \Delta d_j^{(k)} \quad , \quad j = 1,2,\ldots,9 ,$$

$$T^{(k+1)}(P) = \sum_{i=1}^{12} c_i^{(k+1)} \cdot B_i(\Psi_T, P) ,$$

$$V^{(k+1)}(P) = \sum_{i=1}^{9} d_i^{(k+1)} \cdot B_i(\Psi_V, P) ,$$

$$T_S^{(k+1)} = T_S^{(k)} + \Delta T_S^{(k)} ,$$

$$k = k + 1 .$$

Step 8) If $k < 3$ go to Step 2.

Step 9) Output from THAP is

$$T^{(3)}(P),\ T_S^{(3)} \quad \text{and} \quad W^{(3)}(P) = \exp(V^{(3)}(P))$$

for selected pressure levels.

SMHI Rapporter, METEOROLOGI OCH KLIMATOLOGI (RMK)

Nr 1 Thompson, T, Udin, I, and Omstedt, A
Sea surface temperatures in waters surrounding Sweden
Stockholm 1974

Nr 2 Bodin, S
Development on an unsteady atmospheric boundary layer model.
Stockholm 1974

Nr 3 Moen, L
A multi-level quasi-geostrophic model for short range weather predictions
Norrköping 1975

Nr 4 Holmström, I
Optimization of atmospheric models
Norrköping 1976

Nr 5 Collins, W G
A parameterization model for calculation of vertical fluxes of momentum due to terrain induced gravity waves
Norrköping 1976

Nr 6 Nyberg, A
On transport of sulphur over the North Atlantic
Norrköping 1976

Nr 7 Lundqvist, J-E, and Udin, I
Ice accretion on ships with special emphasis on Baltic conditions
Norrköping 1977

Nr 8 Eriksson, B
Den dagliga och årliga variationen av temperatur, fuktighet och vindhastighet vid några orter i Sverige
Norrköping 1977

Nr 9 Holmström, I, and Stokes, J
Statistical forecasting of sea level changes in the Baltic
Norrköping 1978

Nr 10 Omstedt, A, and Sahlberg, J
Some results from a joint Swedish-Finnish sea ice experiment, March, 1977
Norrköping 1978

Nr 11 Haag, T
Byggnadsindustrins väderberoende, seminarieuppsats i företagsekonomi, B-nivå
Norrköping 1978

Nr 12 Eriksson, B
Vegetationsperioden i Sverige beräknad från temperaturobservationer
Norrköping 1978

Nr 13 Bodin, S
En numerisk prognosmodell för det atmosfäriska gränsskiktet grundad på den turbulenta energiekvationen
Norrköping 1979

Nr 14 Eriksson, B
Temperaturfluktuationer under senaste 100 åren
Norrköping 1979

Nr 15 Udin, I, och Mattisson, I
Havsis- och snöinformation ur datorbearbetade satellitdata - en modellstudie
Norrköping 1979

Nr 16 Eriksson, B
Statistisk analys av nederbördsdata. Del I. Arealnederbörd
Norrköping 1979

Nr 17 Eriksson, B
Statistisk analys av nederbördsdata. Del II. Frekvensanalys av månadsnederbörd
Norrköping 1980

Nr 18 Eriksson, B
Årsmedelvärden (1931-60) av nederbörd, avdunstning och avrinning
Norrköping 1980

Nr 19 Omstedt, A
A sensitivity analysis of steady, free floating ice
Norrköping 1980

Nr 20 Persson, C och Omstedt, G
En modell för beräkning av luftföroreningars spridning och deposition på mesoskala
Norrköping 1980

Nr 21 Jansson, D
Studier av temperaturinversioner och vertikal vindskjuvning vid Sundsvall-Härnösands flygplats
Norrköping 1980

Nr 22 Sahlberg, J and Törnevik, H
A study of large scale cooling in the Bay of Bothnia
Norrköping 1980

Nr 23 Ericson, K and Hårsmar, P-O
Boundary layer measurements at Klockrike. Oct. 1977
Norrköping 1980

Nr 24 Bringfelt, B
A comparison of forest evapotranspiration determined by some independent methods
Norrköping 1980

Nr 25 Bodin, S and Fredriksson, U
Uncertainty in wind forecasting for wind power networks
Norrköping 1980

Nr 26 Eriksson, B
Graddagsstatistik för Sverige
Norrköping 1980

Nr 27 Eriksson, B
Statistisk analys av nederbördsdata. Del III. 200-åriga nederbördsserier
Norrköping 1981

Nr 28 Eriksson, B
Den "potentiella" evapotranspirationen i Sverige
Norrköping 1981

Nr 29 Pershagen, H
Maximisnödjup i Sverige (perioden 1905-70)
Norrköping 1981

Nr 30 Lönnqvist, O
Nederbördsstatistik med praktiska tillämpningar
(Precipitation statistics with practical applications)
Norrköping 1981

Nr 31 Melgarejo, J W
Similarity theory and resistance laws for the atmospheric boundary layer
Norrköping 1981

Nr 32 Liljas, E
Analys av moln och nederbörd genom automatisk klassning av AVHRR data
Norrköping 1981

Nr 33 Ericson, K
Atmospheric Boundary layer Field Experiment in Sweden 1980, GOTEX II, part I
Norrköping 1982

Nr 34 Schoeffler, P
Dissipation, dispersion and stability of numerical schemes for advection and diffusion
Norrköping 1982

Nr 35 Undén, P
The Swedish Limited Area Model (LAM). Part A. Formulation
Norrköping 1982

Nr 36 Bringfelt, B
A forest evapotranspiration model using synoptic data
Norrköping 1982

Nr 37 Omstedt, G
Spridning av luftförorening från skorsten i konvektiva gränsskikt
Norrköping 1982

Nr 38 Törnevik, H
An aerobiological model for operational forecasts of pllen concentration in th air
Norrköping 1982

Nr 39 Eriksson, B
Data rörande Sveriges temperaturklimat
Norrköping 1982

Nr 40 Omstedt, G
An operational air pollution model using routine meteorological data
Norrköping 1984

Nr 41 Christer Persson and Lennart Funkquist
Local scale plume model for nitrogen oxides.
Model description.
Norrköping 1984

Nr 42 Stefan Gollvik
Estimation of orographic precipitation by dynamical interpretation of synoptic model data.
Norrköping 1984

Nr 43 Olov Lönnqvist
Congression - A fast regression technique with a great number of functions of all predictors.
Norrköping 1984

Nr 44 Sten Laurin
Population exposure to So and NO_x from different sources in Stockholm.
Norrköping 1984

Nr 45 Jan Svensson
Remote sensing of atmospheric temperature profiles by TIROS Operational Vertical Sounder.
Norrköping 1985

SMHI

SWEDISH METEOROLOGICAL AND HYDROLOGICAL INSTITUTE
S-60176 Norrköping, Sweden. Tel. +46 11 15 80 00. Telex 64400 smhi s.

ISSN 0347-2116